TISSUE ENGINEERING: Part A
Volume 17, Numbers 3 and 4, 2011

DOI: 10.1089/ten.tea.2009.0810

A Microfabricated Scaffold Induces the Spheroid Formation of Human Bone Marrow-Derived Mesenchymal Progenitor Cells and Promotes Efficient Adipogenic Differentiation

Yoshitaka Miyagawa, Ph.D.,[1] Hajime Okita, M.D., Ph.D.,[1] Masami Hiroyama, Ph.D.,[2] Ruriko Sakamoto, M.S.,[2] Maki Kobayashi, M.S.,[2] Hideki Nakajima, Ph.D.,[1] Yohko U. Katagiri, Ph.D.,[1] Junichiro Fujimoto, M.D., Ph.D.,[3] Jun-Ichi Hata, M.D., Ph.D.,[1,4] Akihiro Umezawa, M.D., Ph.D.,[5] and Nobutaka Kiyokawa, M.D., Ph.D.[1]

Here, we report the highly efficient *in vitro* differentiation of human bone marrow-derived mesenchymal stem/progenitor cells (MPCs) using a novel nanotechnology-based culture plate, nanoculture plate® (NCP). The NCP contains uneven microfabrications with diameters of ~2–3 μm arranged in a honeycomb pattern on its culture surface, which is devoid of animal-derived protein sources. When human MPCs were subjected to three-dimensional (3D) culture using an NCP, they rapidly formed adhesive spheroids. We showed that adipogenic differentiation in NCP-mediated 3D cultures led to more rapid accumulation of triglycerides than that in two-dimensional cultures. During adipogenesis in 3D cultures, the rapid and intense induction of adipocyte-specific gene expressions, such as peroxisome proliferator-activated receptor γ (PPAR-γ), CCAAT-enhancer-binding protein α (C/EBP-α), adipocyte protein 2 (aP2), and adiponectin was observed. Together, these results indicate that this 3D culture system is suitable for the differentiation of human MPCs into adipogenic lineage, and could be applicable to adipose tissue engineering under xeno-free condition.

Introduction

HUMAN BONE MARROW contains nonhematopoietic stem/progenitor cells that are known as mesenchymal stem/progenitor cells (MPCs). MPCs maintain the multipotency and can differentiate into various types of cells in mesenchymal linages, such as osteoblasts,[1,2] adipocytes,[3] myocytes,[4] chondrocytes,[5] and cardiomyocytes.[6] Surprisingly, recent reports have suggested that MPCs are able to transdifferentiate into neurogenic cells, including astrocytes,[7] oligodendrocytes, and neurons.[8,9] Because of their multipotency, MPCs are expected to be a plausible cell source for cell therapy and tissue engineering applications. Indeed, human MPC implantation provides symptomatic relief not only in rat models, but also in human patients with myocardial infarction.[10,11] Human MPC implantation is also reportedly useful for the treatment of child with osteogenesis imperfecta.[12] These results indicated the effectiveness of cell therapy using MPCs against some diseases.

On the other hand, studies on tissue engineering using MPCs have been increasing. For example, MPCs are thought to be a useful source for engineering cartilage tissue because they can differentiate into chondrocyte after typical induction with transforming growth factor in a three-dimensional (3D) environment.[13] Ohgushi and coworkers also demonstrated that artificial bone generated from *ex vivo* expanded MPCs could be applied in a clinical setting.[14,15] However, some issues must be resolved for the proper and effective clinical application of MPC-derived tissue engineering. For example, primary human MPCs, as well as other human cells, have a limited life span and lose their expansion and differentiation capabilities after several passages. Differentiation potential of MPCs also decrease depending on the age of the donor. Further, the characteristics of MPCs cultured in conventional two-dimensional (2D) culture dishes or *ex vivo* engineered tissues in 2D culture often differ from those within the living body. In addition, the foreign proteins and antigens used in *ex vivo* cultures and differentiation induction may cause immune rejection. To resolve these problems, *ex vivo* culture conditions and differentiation methods must be optimized for human MPCs.

Cell–cell interactions are crucial for maintaining undifferentiated state in stem cells and for inducing effective *in vitro* differentiation.[16,17] The tissue microenvironment plays a

[1]Department of Pediatric Hematology and Oncology Research, National Research Institute for Child Health and Development, Tokyo, Japan.
[2]SCIVAX Corporation, Kawasaki-shi, Japan.
[3]Clinical Research Center, National Center for Child Health and Development, Tokyo, Japan.
[4]College of Human Science, Tokiwa University, Mito-shi, Ibaraki, Japan.
[5]Department of Reproductive Biology, National Research Institute for Child Health and Development, Tokyo, Japan.

critical role in guiding the differentiation of stem cells during normal regenerative processes.[18,19] Recently, *in vitro* 3D culture methods using various biomaterials have been tested for their applicability to culturing stem cell. In some 3D culture system, cell shape, morphogenesis, motility, gene expression, and signaling are often more closer to those present in organs and tissues *in vivo* than ordinary 2D cultures, and cells in 3D culture can mimic *in vivo* tissue development. Therefore, some materials that would induce proliferating cells to form 3D structure are very useful for the culture and the differentiation of stem cells.

The nanoculture plate® (NCP) is a recently developed plate and basically consists of a textured surface with specific characteristics that induces spheroids formation; this plate contains uneven microfabrications with diameter of ~2–3 μm arranged in a honeycomb pattern on the culture surface. The NCP system can be used to generate uniform adhesive spheroids of cancer cell lines (lung cancer, head and neck carcinoma, glioma, colon cancer, pancreatic cancer, and hepatocellular carcinoma), hepatocytes, and preadipocytes using conventional techniques without any animal compounds (www.scivax.com/cell/english/index.html). NCP-mediated cell spheroids attach to the scaffold of microfabrications on the plate using their pseudopodia, and the primary phenotype of the cells is highly preserved. We referred to this culture system for spheroid formation as 3D culture hereafter. In the present study, we investigated the effect of the 3D environment provided by the NCP system on the differentiation of human MPCs into mesenchymal lineages, especially adipocytes. We show here that NCP-mediated 3D cultures provide human MPCs with favorable conditions needed to maximize their potential for differentiation into mesenchymal lineages.

Materials and Methods

Materials

Three types of 96-well NCPs with a nano-honeycomb pattern [NCP-L-NH (96)], a microhoneycomb pattern [NCP-L-MH (96)], and a microsquare pattern [NCP-L-MS (96)] were provided by SCIVAX Corp.

Cell culture

UET-13 cells (human MPCs with an extended life span using retroviral transduction)[20] were cultured in Dulbecco's modified Eagle's medium with 10% fetal bovine serum at 37°C under a humidified 5% CO_2 atmosphere. For the spheroid formation assay, UET-13 cells were seeded at a density of 5×10^3 cells/100 μL/well using hMSC Adipogenic Differentiation Medium (Lonza) on the three types of 96-well-NCP plates described above. To induce differentiation into adipocytes, the UET-13 cells were seeded at a density of 5×10^3 cells/100 μL/well in hMSC Adipogenic Differentiation Medium (Lonza) and were cultured on a conventional 2D cell culture plate and an NCP. The culture medium was replaced by removing 70 μL of medium and then adding 100 μL of fresh medium every 3 or 4 days. After 8 days of culture, the medium was changed to Adipogenic Maintenance Medium (Lonza) and the culture medium was similarly replaced every 2 days until 14 days. To induce differentiation into osteoblasts, the UET-13 cells were seeded at a density of 1×10^4 cells/100 μL/well in hMSC osteogenic Differentiation Medium (Lonza). The culture medium was replaced in the above-described manner every 3 or 4 days.

Cell attachment assay and cell proliferation/viability assay

UET-13 cells were seeded at a density of 5×10^3 cells/100 μL/well using Dulbecco's modified Eagle's medium with 10% fetal bovine serum and were cultured on a conventional 2D cell culture plate and the NCP-L-NH plate. After 24 h, the medium was recovered and the wells were gently washed with PBS three times. The cells that were recovered in medium and rinse solution, and left attached to the plates were counted by trypan blue dye exclusion assay. Cell attachment efficiency was calculated as the number of cells attached to the plates divided by the total number of viable cells. For cell proliferation/viability assay, UET-13 cells were seeded as described above and the medium was replaced every 3 or 4 days. At days 0, 3, 7, 10, and 14, the cell proliferation and viability were assessed by trypan blue dye exclusion assay. Cell viablity was calculated as the number of viable cells divided by the total number of cells.

Triglyceride and adenosine triphosphate measurements

The culture medium was removed and the cells were collected into tubes containing 25 μL of 0.5 N NaOH/well. The cells were completely lysed by shaking the tubes for 4 h, and the triglyceride (TG) concentration was measured using 4 μL of lysate with a TG E-test Wako (Wako). To normalize the TG contents, the cell number was determined by measuring the adenosine triphosphate concentration using the CellTiter-Glo luminescent cell viability assay (Promega). After the complete lysis of the cells by the addition of 5 μL of Nanoculture lysis® (SCIVAX Corp.) to the culture medium, followed by pipetting, 50 μL of the lysate was mixed with an equal volume of CellTiter-Glo reagent and the luminescence was measured using a luminometer after incubation.

TG staining of the cells that had differentiated into adipocytes

Cells were washed with PBS, and then stained using AdipoRed (BioWhittaker Inc.) and observed using fluorescence microscopy. For Oil-red O staining, the cells were fixed with 10% formalin for 1 h and soaked in 3 mg/mL of Oil-red O in 60% isopropanol for 20 min, then washed with 60% isopropanol. After washing twice with H_2O, the cells were observed using a phase-contrast microscope.

Alizarin Red staining of the cells that had differentiated into osteoblasts

Cells were fixed with 10% formalin for 20 min and washed with H_2O twice and then stained with 0.1% (w/v) Alizarin Red solution (Wako). After washing twice with H_2O, the cells were observed using a phase-contrast microscope.

Real-time reverse transcriptase-polymerase chain reaction analysis

Total RNA was extracted from the cells using ISOGEN (Nippon Gene Co., Toyama, Japan) and reverse transcribed

using First-Strand cDNA Synthesis Kit (GE Healthcare Bio-Science Corp.). Real-time reverse transcriptase polymerase chain reaction (RT-PCR) was performed using FastStart Universal SYBR Green Master (ROX) (Roche Diagnostics), TaqMan® Universal PCR Master Mix and TaqMan Gene Expression Assays, Inventoried assay on an ABI PRISM® 7900HT Sequence Detection System (Applied Biosystems), according to the manufacturer's instructions. The human glyceraldehyde 3-phophate dehydrogenase gene was used as an internal control for normalization. The sequences of the gene specific primers for real-time RT-PCR were as follows: peroxisome proliferator-activated receptor γ (PPAR-γ), 5′-GACCTGAAAC TTCAA GAGTA CCAAA −3′ and 5′-TGAGGCTTAT TGTAGAGCTG AGTC −3′; CCAAT-enhancer-binding protein α (C/EBP-α), 5′-GCAAATCGTG CCTTGTCAT −3′ and 5′-CTCATGGGGG TCTGCTGTAG −3′; adipocyte protein 2 (aP2), 5′-CCTTT AAAAA TACTGAGATT TCCTTCA −3′ and 5′-GGACACC CCCATCTAAGGTT −3′; Adiponectin, 5′-AGAGATGGCA CCCCTGGT −3′ and 5′-CACCGATGTC TCCCTTAGGA −3′.

DNA microarray analysis

The total RNA isolated from cells was reverse transcribed and labeled using one-cycle target labeling and control reagents as instructed by the manufacturer (Affymetrix). The labeled probes were hybridized to a Human Genome U133 Plus 2.0 Array (Affymetrix). The arrays were performed and analyzed using GeneChip Operating Software 1.2 (Affymetrix). Background subtraction, normalization,[21] and gene ontology (GO) analysis were performed using GeneSpring GX 10. 0. 1 software (Agilent Technologies). The data were filtered by eliminating genes with a signal intensity of lower than 100. The signal value for each transcript was normalized to the median of the control sample (undifferentiated UET-13 cells). To determine whether genes were differentially expressed between the 2D and 3D cultures, the fold change was calculated between the 2D and 3D cell cultures and genes with a fold change ≥ 2 were identified. In the tables, the relative mRNA levels are presented using a logarithmic scale.

Microscopy

Fluorescent and phase-contrast cell images were observed using a microscope (Nikon Eclipse TS100, Nikon; objective lens magnification, ×20). Scanning electron microscopy (SEM) images were obtained using a JSM-6060 SEM (Jeol), equipped with a high-efficiency in-lens detector, typically with an electron energy of 5 or 10 kV. The scale indicates 10 μm.

Statistical analysis

Data are expressed as mean values with corresponding standard deviations. To evaluate the difference in 2D and 3D culture, the Student's *t*-test was applied. $p < 0.05$ was considered as a statistically significant difference between the two groups.

Results

Microfabricated structures on NCP and spheroid formation of UET-13 cells

In this study, we used UET-13 cells as a human MPC model.[20,22] UET-13 cells were obtained by prolonging the lifespan of human bone marrow stromal cells using retroviral transduction, and these cells retained their ability to differentiate into not only mesodermal derivatives but also neuronal progenitor-like cells. To investigate the effect of nanotechnology-based microfabrications as a scaffold for the *in vitro* growth and differentiation of human MPCs, UET-13 cells were cultured on NCP and compared with those cultured with conventional 2D culture plate. First, to test which type of NCP was optimal for the spheroid formation of hMPCs, UET-13 cells were cultured on three types of NCPs (NCP-L-NH, -MH, and -MS). SEM imaging revealed that each type of NCP had a uniform pattern (Fig. 1A). These plural polygonal (honeycomb and square) patterns expanded sequentially across the plane creating an uneven surface. After 1 day of 3D culture, the UET-13 cells had migrated and self-assembled, forming multiple adhesive spheroids (Fig. 1B). In contrast, they did not form spheroids when they were cultured on conventional 2D culture plates (referred to as 2D culture hereafter). The spheroids formed on NCP-L-NH were larger and had smooth contour. Therefore, we used NCP-L-NH for the culture of UET-13 cells in the subsequent experiments (referred to as 3D culture hereafter).

NCP-L-NH effectively induces osteogenic and adipogenic differentiation in UET-13 cells

First, we evaluated the cytocompatibility of NCP-L-NH plate. After 1 day of culture, the spheroids are weakly attached to the textured surface in the NCP plate. These spheroids tend to detach from the culture surface by gentle wash with PBS. The proportion of the attached cells in the NCP plate was lower than that in 2D culture (Fig. 2A). Next, we assessed cell proliferation and viability in the NCP plates by trypan blue dye exclusion assay. Figure 2B showed that UET-13 cells grew slowly for first 3 days and then grew exponentially on the textured surface. Then, we evaluated the cell viability of UET-13 cells. Figure 2C shows that the most UET-13 cells were viable in the NCP plates as well as in the 2D cultures. These results indicate that the NCP-L-NH plates are cytocompatible and the UET-13 cells proliferate slowly but normally on the microfabrications.

We next tested the effect of a 3D culture using NCP-L-NH on the efficiency of the differentiation of UET-13 cells. First, the effect of NCP on differentiation into an osteogenic lineage was examined. When UET-13 cells were induced to undergo osteogenic differentiation in NCP, as shown in Figure 3A, the intensity of the Alizarin Red S staining was stronger than that observed for 2D culture. We next tested the effect of NCP on adipogenic development. During the adipogenic differentiation of UET-13 cells, more lipid droplets accumulated on the cell surfaces in the 3D cultures (Fig. 3B), compared with the accumulation observed in 2D cultures. Further, AdipoRed staining clearly showed a greater accumulation of intracellular TG in the cell spheroids of UET-13 cells (Fig. 3C). The quantitative determination of TG accumulation indicated that TG accumulation in the 3D cultures was greater than those in the 2D cultures (Fig. 3D).

Rapid increase in adipocyte-related gene expression in UET-13 cells during adipogenic differentiation in 3D culture using NCP

To examine the effect of 3D culture using NCP on gene expression underlying the adipogenic differentiation of

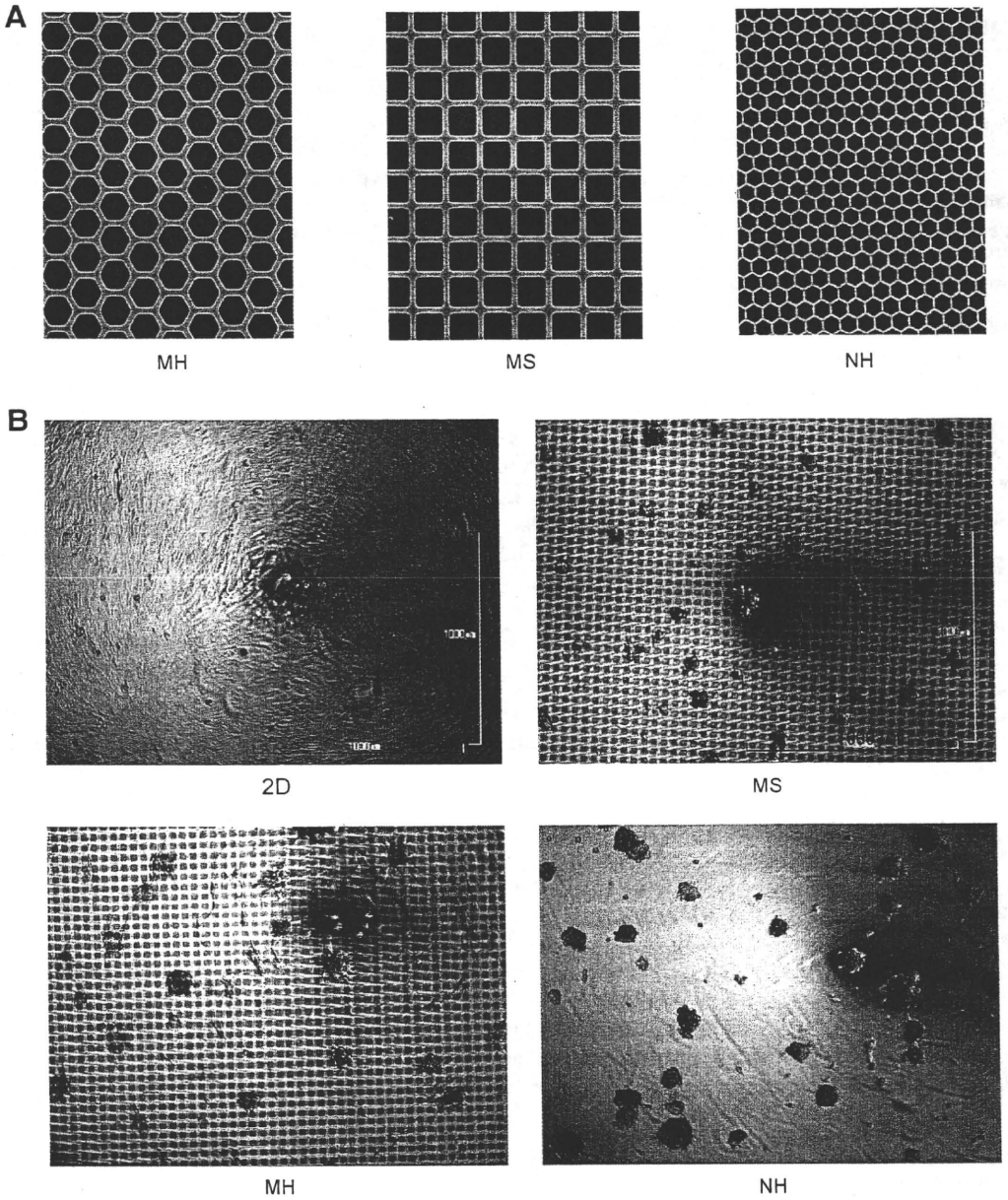

FIG. 1. Spheroid formation of UET-13 cells in nanoculture plate® (NCP)-mediated three-dimensional (3D) culture. **(A)** Scanning electron microscopy images of microfabrications in NCP: microhoneycomb (MH); microsquare (MS); nanohoneycomb (NH). **(B)** Spheroid formation of UET-13 cells. The cells were cultivated for 1 day on a two-dimensional (2D) plate or the indicated NCP.

human MPCs, the mRNA levels of adipocyte marker genes were monitored during adipogenic differentiation. In 3D culture, a remarkable elevation in the PPAR-γ and adiponectin mRNA levels was observed (<7-fold and <10-fold, respectively) after 3 days of adipogenic differentiation, whereas only a faint enhancement (<2-fold) was observed in 2D cultures (Fig. 4A, B). The C/EBP-α mRNA levels were markedly elevated after 3 days of adipogenic differentiation in both 2D and 3D cultures, and the level in 3D cultures represented the maximum value (Fig. 4C). Similar to C/EBP-α, the aP2 mRNA levels increased markedly over time in both the 2D and 3D cultures; however, that in the 3D cultures increased more rapidly than that in the 2D cultures (Fig. 4D).

To further investigate the differences in the molecular basis of adipogenesis, we compared the gene expression profiles of UET-13 cells during adipogenic differentiation in 2D and 3D culture using Affymetrix Genechip technology. To identify genes that were differentially expressed in 2D and 3D cultures, a threshold of a twofold change in gene expression was used as the cut-off value after background subtraction and normalization. We determined that the expression levels of 686 genes differed significantly between 2D and 3D cultures after adipogenic differentiation (upregulation of 333 genes and downregulation of 353 genes in 3D cultures) (Supplementary Tables 1 and 2; Supplementary Data are available online at www.liebertonline.com/ten). We further analyzed the genes with different expression levels in

2D and 3D cultures after differentiation using a GO analysis. These genes and their expression levels relative to the control (undifferentiated UET-13 cells) are shown using a log scale in Supplementary Tables 3 and 4. As expected, genes that were downregulated in 3D cultures were significantly overrepresented in some GO gene sets associated with cell adhesion, extracellular matrix (ECM), and cytoskeleton, such as cell adhesion, collagen, ECM, actin binding, actin cytoskeleton, and cytoskeleton. In particular, the expression pattern of the collagen family differed between 2D and 3D cultures (Supplementary Tables 3 and 4). In 3D cultures, COL14A1, COL18A1, and COL7A1 were highly expressed in UET-13 cells, whereas the expression levels of COL11A1, COL12A1, COL1A1, COL1A2, COL5A1, COL5A2, and COL8A1 decreased. Interestingly, collagen type XVIII, which is highly expressed during adipogenic differentiation (gene symbol: COL18A1),[23,24] was upregulated, whereas collagen type I (gene symbol: COL1A1 and COL1A2), which is abundant in bone and fibrous tissues, was downregulated in 3D cultures (Supplementary Table 4). Moreover, expression of ECM degradation enzyme, the matrix metallopeptidase (MMP) family (including MMP1, MMP3, MMP7, MMP14, and MMP19), and a tissue inhibitor of metallopeptidase, TIMP3, were upregulated in 3D culture. In addition, expression of some lineage specific marker genes were lower in 3D cultures, including ALPL, DKK1, RUNX2, MAP2, NEFL, NEGR1, and SOX4 (Supplementary Tables 1 and 2).

Next, we focused on adipocyte-related genes such as adipocytokine, and examined changes in the expression patterns. The microarray analysis identified genes that were commonly upregulated in both 2D and 3D culture but that were more efficiently upregulated in 3D culture, including genes associated with the ECM and cytoskeleton (ADAM17, TIMP1, and TIMP4), transcriptional regulators (CEBPA, PPARA, and PPARGC1A), signal transduction molecules (PRKAA1, STAT5A, and STAT5B), cytokines (IL1R1, IL23A, IL6R, and INSR) and other adipose differentiation related genes (ADFP, AGTR1, ANGPTL2, ANGPTL4, BCL2L1, CAMKK1, CST3, and HSD11B1) (Supplementary Table 5). In contrast, genes that were commonly downregulated in both 2D and 3D cultures but that more efficiently downregulated in 3D cultures were also identified, including genes associated with signal transduction (MIF, PDGFA, PDGFC, PPKACA, SMAD3, and STAT1) and cytokines and chemokines (CCL2, EGFR, FGF2, LOX, MIF, and SERPINE1). Interestingly, expression of some genes was differentially regulated in 2D and 3D cultures. Some genes were upregulated in 3D cultures and downregulated in 2D cultures after differentiation, including genes associated with the ECM and cytoskeleton (MMP2, TIMP2, TIMP3, and TLR4), transcription (CEBPB), and other adipose differentiation related genes (CSF1, EREG, IGFBP1, IGFBP3, PHLDA1, SOCS3,

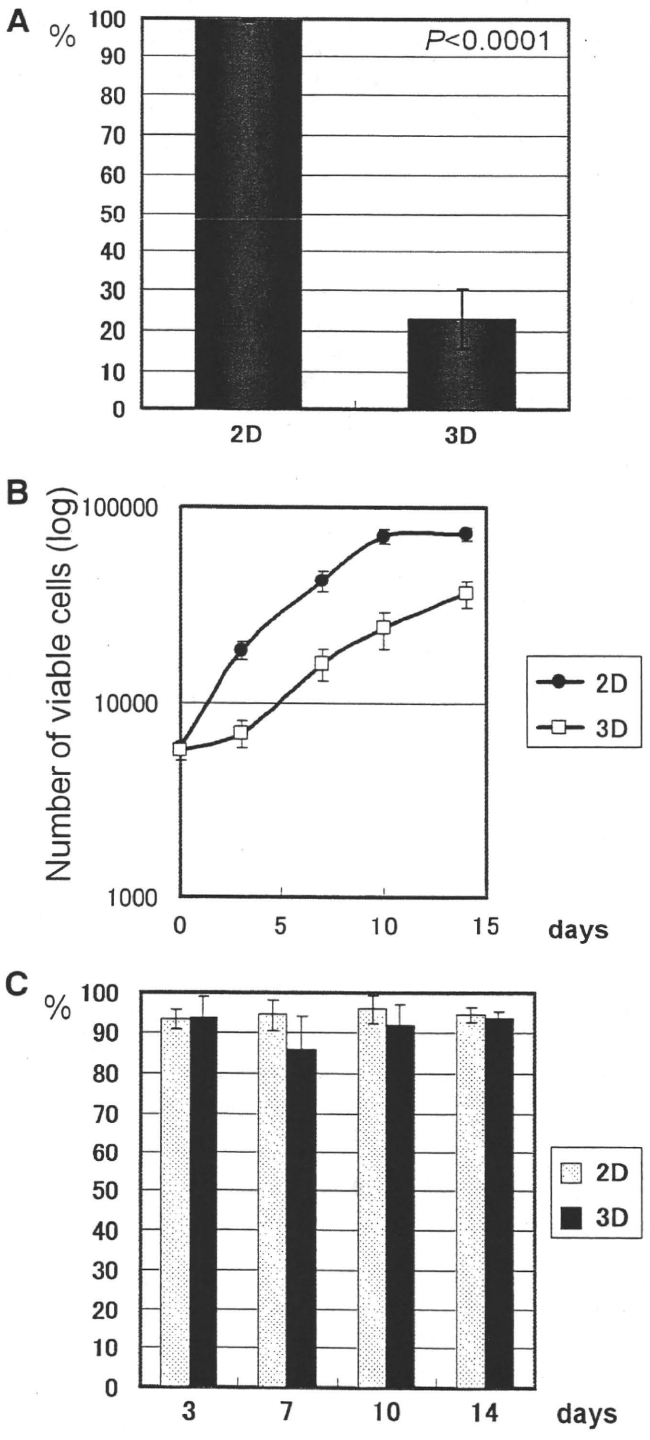

FIG. 2. Cytocompatibility of NCH-L-NH. **(A)** UET-13 cells were seeded on conventional 2D culture wells and NCP-L-NH. Cell attachment efficiency was calculated as the number of cells attached to the plates after 24 h divided by the total number of viable cells. Data were expressed as mean value of triplicate wells with SD. The proportion of attached cells on the NCP plate (3D) was significantly lower than that in 2D culture ($p < 0.0001$). **(B)** Trypan blue dye exclusion assay was used to evaluate the cell proliferation. UET-13 cells were seeded at a density of 5×10^3 cells/100 μL/well. Numbers of the cells were counted by trypan blue dye exclusion assay at days 0, 3, 7, 10, and 14. Data were expressed as mean value of triplicate wells with SD. The numbers of the cells in 3D culture in each time point (days 0, 3, 7, 10, and 14) were significantly smaller than that in 2D culture ($p < 0.002$). **(C)** Cell viability of UET-13 cells. The percentage of viable cells was evaluated by trypan blue dye exclusion assay. Data were expressed as mean value of triplicate wells with SD. The differences between 2D and 3D culture were not significant ($p > 0.05$)

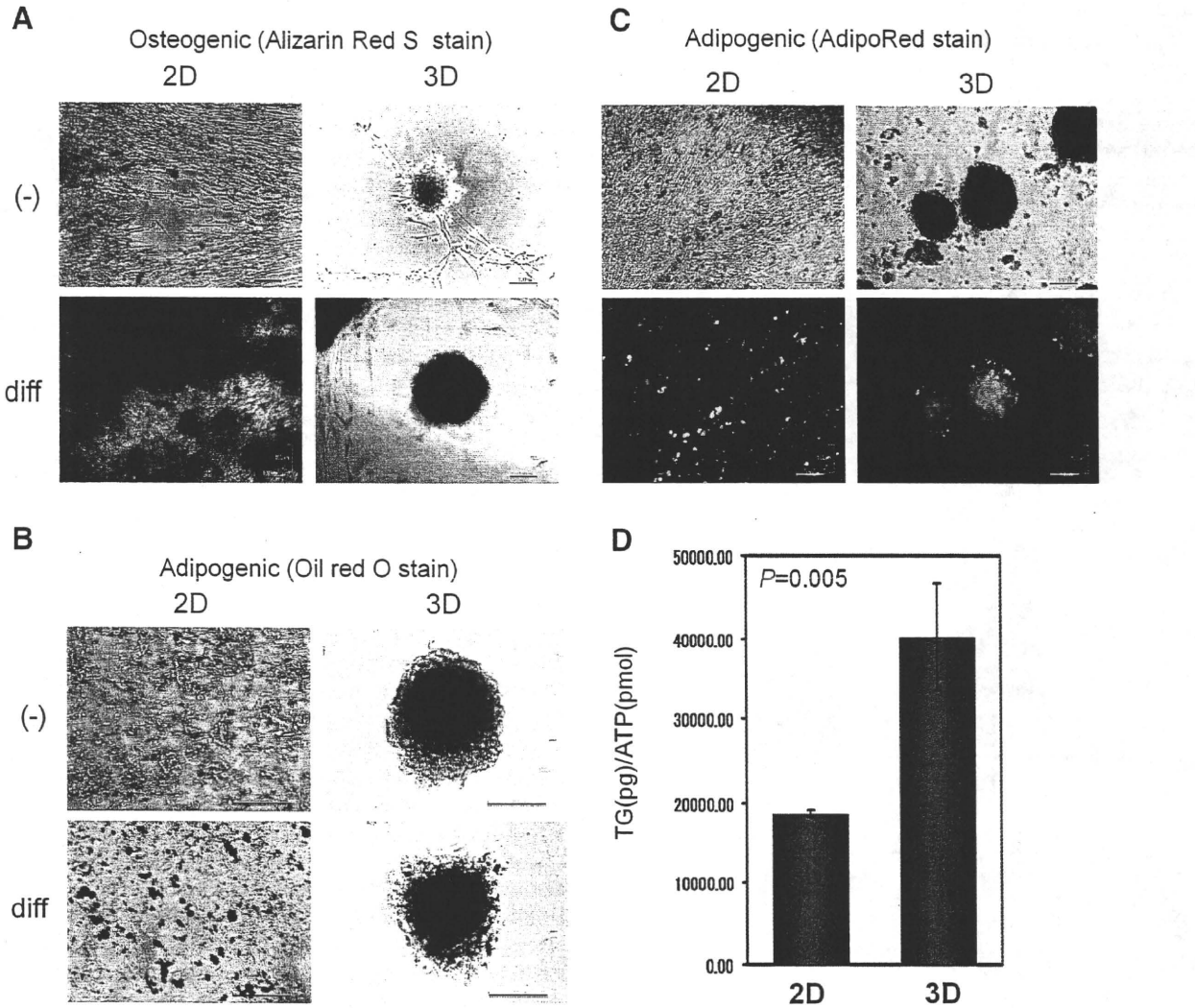

FIG. 3. Differentiation of UET-13 cells into mesenchymal lineages in 2D and 3D cultures. **(A)** Osteogenic differentiation of UET-13 cells in 2D and 3D culture. Cells were incubated in hMSC osteogenic Differentiation Medium for 14 days and stained with Alizarin Red. **(B, C)** Adipogenic differentiation of UET-13 cells in 2D and 3D cultures. Cells were incubated in hMSC adipogenic Differentiation Medium for 8 days and stained with Oil Red O **(B)** or Adipo Red (**C**). The scale bar indicates 100 μm. **(D)** Triglyceride measurements after adipogenic differentiation in UET-13 cells in 2D and 3D cultures. UET-13 cells were incubated in hMSC Adipogenic Differentiation Medium for 8 days and then lysed; the amount of triglyceride was measured. The signal intensities were normalized using the adenosine triphosphate (ATP) concentration. Data are the relative values with the SD of triplicate wells on one experience. Statistically significant difference between 2D and 3D culture at $p = 0.005$ was observed.

TNFRSF1B, and UCP2). Other genes were upregulated in 2D cultures and downregulated in 3D cultures after differentiation, including transcriptional regulator (HIF1A) and adipocytokines (CXCL12, F3, FAS, IGF2, PTX3, SPARC, THBS1, and THBS2).

Discussion

In this study, we tested the effectiveness of NCP as a scaffold for human MPCs during *in vitro* differentiation into mesenchymal lineage, including osteogenic and adipogenic lineages. Compared with conventional 2D cultures, 3D cultures using NCP clearly promoted the differentiation of human MPCs into osteogenic and adipogenic lineages. These results indicated that NCP could serve as an excellent scaffold for human MPCs during *ex vivo* differentiation.

The UET-13 mesenchymal progenitor cells effectively formed adhesive spheroids in the NCP plates. In conventional culture plates, the cells firmly attach to the culture surface and grow as monolayers. The surface material of NCP is nonadhesive synthetic resin, but the microfabricated structure would enable cells to adhere to the plates with cell projections.[25] This cell–plate adhesion would be weaker than cell–cell adhesion, and this low cell–plate adhesion could promote spheroid formation.

To find an appropriate scaffold for the *in vitro* culture and differentiation of human MPCs, various materials have been tested, including collagen,[26] silk,[27] chitosan,[28] Engelbreth-Holm-Swarm-derived gel, Pluronic F-127 hydrogel,[29] atelocollagen,[30] poly(ethylene glycol) diacrylates hydrogels,[31] poly(-caprolactone),[32] nonwoven poly(ethylene terepthalate)

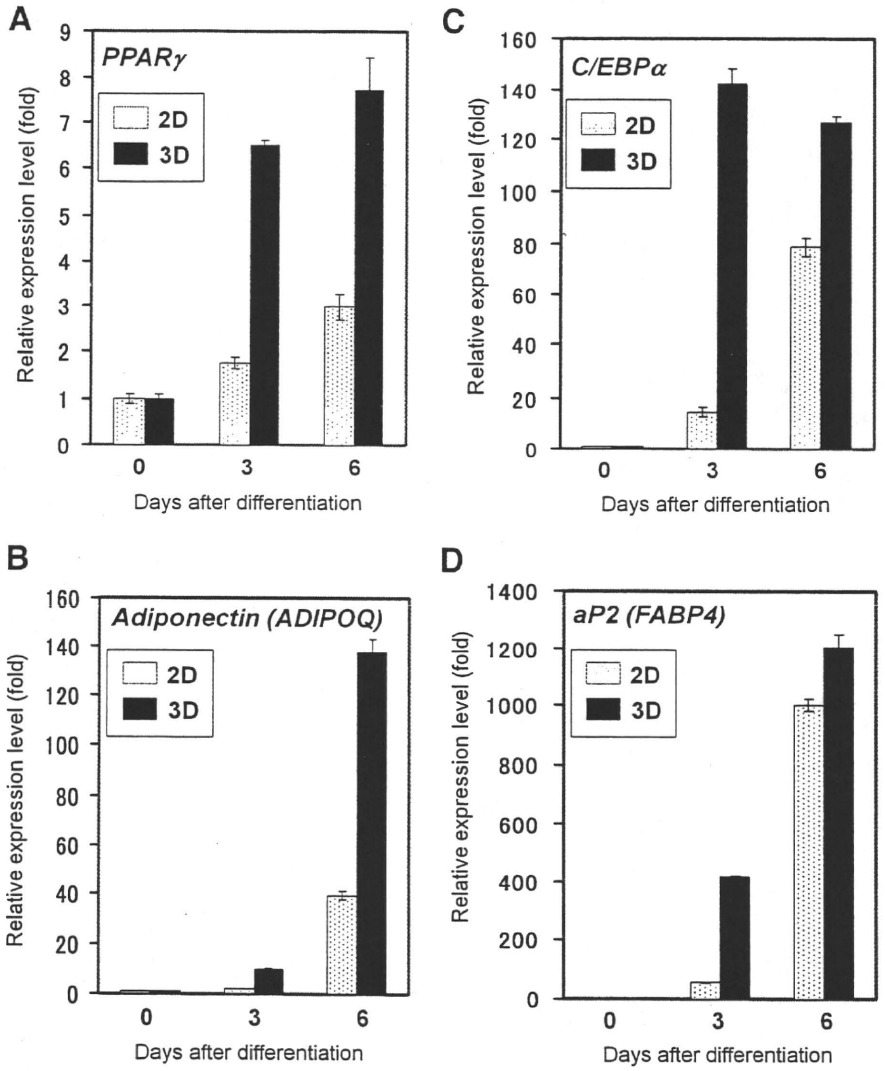

FIG. 4. Changes in expression levels of adipogenic marker genes after adipogenic differentiation in UET-13 cells. Real-time reverse transcriptase-polymerase chain reaction was performed to investigate expression of **(A)** peroxisome proliferator-activated receptor γ (PPAR-γ), **(B)** adiponectin, **(C)** CCAAT-enhancer-binding protein α (C/EBP-α), and **(D)** adipocyte protein 2 (aP2). The signal intensities were normalized using those of a control housekeeping gene (human glyceraldehyde 3-phophate dehydrogenase gene). Data were the relative values with the SD of triplicate wells and normalized to the mRNA level at 0 h, which was arbitrarily set to 1 in the graphical presentation.

fibrous matrices,[33] and thermoreversible gelation polymer.[34] However, these materials are too complicated to manipulate. Further, in some *in vitro* 3D culture systems, animal and chemical substances present in the culture system might stimulate cells and induce changes in the primary phenotypes. In contrast, the handling of NCP 3D culture system was comparatively easy. The UET-13 cells were seeded conventionally and they easily formed adhesive spheroids in the 3D cultures. In addition, the NCP-mediated 3D culture system does not contain animal substances. Therefore, NCP could be useful for studying cellular properties and the development of tissue engineering applications for human MPCs under xeno-free condition.

In the present study, NCP enabled human MPCs to form 3D adhesive spheroids and enhanced their osteogenic and adipogenic differentiation potential. Unlike our results using NCP, a TiO_2-derived microfabricated scaffold did not enable rat MPCs to form a 3D structure.[35] However, the previous authors concluded that TiO2-mediated microfabrication could stimulate cellular responses and enhance the assembly of integrin and actin fibers, as well as nuclear signaling. These differences suggest that the formation of a 3D structure and the cell phenotype might depend on the materials and the microfabrication pattern of the scaffold. To efficiently control the differentiation and proliferation of human MPCs, the materials and microfabrication pattern should be optimized for intended purposes.

As shown in the global gene expression analysis, a group of genes related to ECM, cell adhesion, and the cytoskeleton was more efficiently expressed in 3D cultures (Supplementary Tables 3 and 4). In agreement with this result, the use of both natural and synthetic biomaterials as 3D scaffolds generally induces changes in the expression patterns of cell adhesion and ECM-related genes. In addition, NCP-mediated 3D cultures induce changes in the ECM production pattern not only by changing expression of ECM components, such as member of the collagen family and the laminin family (LAMA1 sand LAMB3), but also by increasing expression of ECM degradation enzymes, including member of the MMP family (Supplementary Table 3). ECM remodeling is essential for adipocyte differentiation, and the inhibition of MMP-mediated ECM remodeling prevents adipocyte differentiation.[36] The dynamic change in ECM-related gene expression induced by NCP might promote ECM remodeling, and stimulating cell assembly

and the formation of the spheroids. The cell–cell interaction induced by the resultant spheroids might in turn enhance the cellular responses and nuclear signaling, and influencing the differentiation potential. Indeed, the upregulated genes in the 3D cultures were also statistically significantly overrepresented in some GO gene sets associated with "response to external stimulus" and "response to wounding" (data not shown).

As shown in Figure 4, master regulator genes for adipogenic differentiation, such as PPARγ and C/EBP-α, were significantly expressed in 3D cultures. The induction of these genes is preceded by that of C/EBP-β and C/EBP-δ.[37] In 3D cultures, the upregulation of C/EBP-β was already observed at 72 h, whereas it was not observed in 2D cultures at this time point (Supplementary Table 5). The expression levels of PPARγ downstream genes such as FABP3, aP2 (FABP4), and LPL were also higher in 3D cultures than in 2D cultures (Supplementary Tables 1, 2, and 5). On the other hand, expression of some adipocytokines, including SPARC, THBS1, and THBS2, was reportedly decreased after differentiation into mature adipocytes.[38] Expression of those genes was downregulated in 3D cultures using NCP. Thus, our results indicated that adipogenic differentiation in 3D cultures accurately mimicked the transcriptional changes that occur in *in vivo* adipogenic cells, compared with the changes 2D cultures. This rapid and accurate transcriptional regulation may be caused by a microfabrication-mediated stimulus, followed by rapid morphological change and oil drop deposition.

In summary, the NCP system may be a useful tool as a scaffold for the *in vitro* differentiation of human MPCs into mesenchymal lineages. The microfabricated scaffold of NCP induced changes in the expression patterns of genes related to cell adhesion, the ECM, and cell–cell interactions, preceded by the rapid induction of transcriptional regulators for adipogenesis. This system would be useful for the development of regenerative medical techniques for mesenchymal tissues, including bone and adipose tissue.

Acknowledgments

This work was supported in part by Health and Labour Sciences Research Grants (the 3rd Term Comprehensive 10-Year-Strategy For Cancer Control H19-010 and H22-011, Research on Children and Families H21-005 and H19-003, Research on Human Genome Tailor made and Research on Publicly Essential Drugs and Medical Devices H18-005) and a Grant-in Aid for Scientific Research (JSPS. KAKENHI 22790366). This work was also supported by CREST, JST, a grant from the Japan Health Sciences Foundation for Research on Publicly Essential Drugs and Medical Devices. Y. Miyagawa is an Awardee of a Research Resident Fellowship from the Foundation for Promotion of Cancer Research (Japan) for the 3rd Term Comprehensive 10-Year-Strategy for Cancer Control.

We respectfully thank Y. Toda for her secretarial work, and M. Itagaki for many helpful discussions and support.

Disclosure Statement

No competing financial interests exist.

References

1. Bruder, S.P., Jaiswal, N., and Haynesworth, S.E. Growth kinetics, self-renewal, and the osteogenic potential of purified human mesenchymal stem cells during extensive subcultivation and following cryopreservation. J Cell Biochem **64,** 278, 1997.
2. Jaiswal, N., Haynesworth, S.E., Caplan, A.I., and Bruder, S.P. Osteogenic differentiation of purified, culture-expanded human mesenchymal stem cells *in vitro*. J Cell Biochem **64,** 295, 1997.
3. Nuttall, M.E., Patton, A.J., Olivera, D.L., Nadeau, D.P., and Gowen, M. Human trabecular bone cells are able to express both osteoblastic and adipocytic phenotype: implications for osteopenic disorders. J Bone Miner Res **13,** 371, 1998.
4. Wakitani, S., Saito, T., and Caplan, A.I. Myogenic cells derived from rat bone marrow mesenchymal stem cells exposed to 5-azacytidine. Muscle Nerve **18,** 1417, 1995.
5. Pittenger, M.F., Mackay, A.M., Beck, S.C., Jaiswal, R.K., Douglas, R., Mosca, J.D., Moorman, M.A., Simonetti, D.W., Craig, S., and Marshak, D.R. Multilineage potential of adult human mesenchymal stem cells. Science **284,** 143, 1999.
6. Makino, S., Fukuda, K., Miyoshi, S., Konishi, F., Kodama, H., Pan, J., Sano, M., Takahashi, T., Hori, S., Abe, H., Hata, J., Umezawa, A., and Ogawa, S. Cardiomyocytes can be generated from marrow stromal cells *in vitro*. J Clin Invest **103,** 697, 1999.
7. Kopen, G.C., Prockop, D.J., and Phinney, D.G. Marrow stromal cells migrate throughout forebrain and cerebellum, and they differentiate into astrocytes after injection into neonatal mouse brains. Proc Natl Acad Sci USA **96,** 10711, 1999.
8. Sanchez-Ramos, J., Song, S., Cardozo-Pelaez, F., Hazzi, C., Stedeford, T., Willing, A., Freeman, T.B., Saporta, S., Janssen, W., Patel, N., Cooper, D.R., and Sanberg, P.R. Adult bone marrow stromal cells differentiate into neural cells *in vitro*. Exp Neurol **164,** 247, 2000.
9. Zhao, L.R., Duan, W.M., Reyes, M., Keene, C.D., Verfaillie, C.M., and Low, W.C. Human bone marrow stem cells exhibit neural phenotypes and ameliorate neurological deficits after grafting into the ischemic brain of rats. Exp Neurol **174,** 11, 2002.
10. Chen, S.L., Fang, W.W., Qian, J., Ye, F., Liu, Y.H., Shan, S.J., Zhang, J.J., Lin, S., Liao, L.M., and Zhao, R.C. Improvement of cardiac function after transplantation of autologous bone marrow mesenchymal stem cells in patients with acute myocardial infarction. Chin Med J (Engl) **117,** 1443, 2004.
11. Davani, S., Marandin, A., Mersin, N., Royer, B., Kantelip, B., Herve, P., Etievent, J.P., and Kantelip, J.P. Mesenchymal progenitor cells differentiate into an endothelial phenotype, enhance vascular density, and improve heart function in a rat cellular cardiomyoplasty model. Circulation **108 Suppl 1,** II253, 2003.
12. Pountos, I., Corscadden, D., Emery, P., and Giannoudis, P.V. Mesenchymal stem cell tissue engineering: techniques for isolation, expansion and application. Injury **38 Suppl 4,** S23, 2007.
13. Chung, C., and Burdick, J.A. Engineering cartilage tissue. Adv Drug Deliv Rev **60,** 243, 2008.
14. Kotobuki, N., and Ohgushi, H. [Repair of arthritic lesions using cultured mesenchymal cells and artificial joints]. Nippon Rinsho **63 Suppl 1,** 680, 2005.
15. Ohgushi, H., Kotobuki, N., Funaoka, H., Machida, H., Hirose, M., Tanaka, Y., and Takakura, Y. Tissue engineered ceramic artificial joint—ex vivo osteogenic differentiation of

Neuroblastoma cells can be classified according to glycosphingolipid expression profiles identified by liquid chromatography-tandem mass spectrometry

TOMONORI KANEKO[1,2], HAJIME OKITA[1], HIDEKI NAKAJIMA[1], KAZUTOSHI IIJIMA[1], NAO OGASAWARA[1,2], YOSHITAKA MIYAGAWA[1], YOHKO U. KATAGIRI[1], ATSUKO NAKAGAWA[3], NOBUTAKA KIYOKAWA[1], TOSHINORI SATO[2] and JUNICHIRO FUJIMOTO[4]

[1]Department of Pediatric Hematology and Oncology Research, National Research Institute for Child Health and Development, Setagaya-ku, Tokyo 157-8535; [2]Department of Biosciences and Informatics, Keio University, Yokohama 223-8522; [3]Division of Diagnostic Pathology, National Medical Center for Children and Mothers; [4]Clinical Research Center, National Center for Child Health and Development, Setagaya-ku, Tokyo 157-8535, Japan

Received April 9, 2010; Accepted June 14, 2010

DOI: 10.3892/ijo_00000779

Abstract. It is hoped that the gangliosides contained in neuroblastomas (NBs) can be used as outcome predictors. We used liquid chromatography-tandem mass spectrometry (LC-MS) to analyze the gangliosides expressed in 11 NB cell lines. LC-MS analysis detected a number of gangliosides, including acetylated forms, with significantly higher sensitivity than conventional high-performance thin-layer chromatography analysis, and the results revealed that the expression profiles of the gangliosides GD1a, GD2, and acetylated GD2 differed according to the NB cell line. Hierarchical clustering based on the ganglioside expression profiles obtained by LC-MS analysis revealed that the NB cell lines could be classified into three types according to their expression of these three gangliosides: A-type characterized by high expression of GD1a and low or no expression of GD2/acetylated GD2, B-type characterized by low or no expression of GD1a and high expression of GD2/acetylated GD2, and AB-type characterized by expression of both GD1a and GD2/acetylated GD2. Interestingly, all three *MYCN* non-amplified cell lines were classified into the A-type. The classification was found to be correlated with mRNA expression of ganglioside synthase and neural-differentiation-related genes. The results of this study indicate that LC-MS analysis is useful as a tool for glycosphingolipid research on malignancies.

Correspondence to: Dr Nobutaka Kiyokawa, Department of Pediatric Hematology and Oncology Research, National Research Institute for Child Health and Development, 2-10-1, Okura, Setagaya-ku, Tokyo 157-8535, Japan
E-mail: nkiyokawa@nch.go.jp

Abbreviations: BSA, bovine serum albumin; *CHGA, chromogranin A*; EIC, extracted ion chromatogram; ESI, Electrospray ionization; GM2, GalNAcß1-4(NeuAcα2-3)Galb1-4GlcCer; GD1a, NeuAcα2-3Galb1-3GalNAcß1-4(NeuAcα2-3)Galß1-4GlcCer; GD1b, Galß1-3GalNAcß1-4(NeuAcα2-8NeuAcα2-3)Galß1-4GlcCer; GD2, GalNAcß1-4(NeuAcα2-8NeuAcα2-3)Galß1-4GlcCer; GD3, NeuAcα2-8NeuAcα2-3Galß1-4GlcCer; GM1a, Galß1-3(NeuAcα2-6)GalNAcß1-4Galß1-4GlcCer; GM3, NeuAcα2-3Galß1-4GlcCer; GQ1b, NeuAcα2-8NeuAcα2-3Galß1-3GalNAcß1-4(NeuAcα2-8NeuAcα2-3)Galß1-4GlcCer; GT1a, NeuAcα2-8NeuAcα2-3Galß1-3GalNAcß1-4(NeuAcα2-3)Galß1-4GlcCer; GT1b, NeuAcα2-3Galß1-3GalNAcß1-4(NeuAcα2-8NeuAcα2-3)Galß1-4GlcCer; Ac-GD2, acetylated GD2; HPTLC, high-performance thin-layer chromatography; HRP, horseradish peroxidase; IT, ion trap; LC-MS, liquid chromatography in combination with mass-spectrometry; mAb, monoclonal antibody; MS/MS, tandem mass spectrometry; *MYCN, v-myc myelocytomatosis viral related oncogene*; *N-CAD, N-cadherin*; *NCAM, neural cell adhesion molecule*; *NB, neuroblastoma*; *NF-H, neurofilament 200 kDa subunit*; *NF-M, neurofilament 160 kDa subunit*; *PBS, phosphate-buffered saline*; *Phox2a, paired-like (aristaless) homeobox 2a*; *Phox2b, paired-like homeobox 2b*; *PTN, pleiotrophin*; RT-PCR, reverse transcription-PCR; *TrkA, neurotrophic tyrosine kinase, receptor, type 1*; *TrkC, neurotrophic tyrosine kinase, receptor, type 3*

Key words: glycosphingolipid, neuroblastoma, LC-MS

Introduction

Ganglioside molecules consist of a sialic acid-containing hydrophilic oligosaccharide chain and a hydrophobic lipid anchor ceramide, and they are embedded in the outer leaflet of the plasma membrane and involved in various cellular processes (1). As summarized in Fig. 1, ganglioside biosynthesis occurs in a series of stepwise glycosylations via two main pathways. One pathway results in the synthesis of GM2, GM1a, GD1a and GT1a (referred to as pathway a in this report), and the other pathway results in the synthesis of GD3, GD2, GD1b, GT1b and GQ1b (referred to as pathway b in this report). Both pathways proceed from a common precursor, GM3, which is derived from lactosylceramide (2). Analogous steps in biosynthesis pathways a and b are catalyzed by the same glycosyltransferases (Fig. 1) (1). Some

gangliosides are expressed aberrantly in many types of tumors and are related to the malignant behavior of their cells (3). Research on oligosaccharide chains, however, has not progressed very far because of a lack of effective methods of analyzing oligosaccharide chains. For example, high-performance thin-layer chromatography (HPTLC), a commonly used method to analyze the ganglioside composition of cells, requires large samples and has limited sensitivity for ganglioside detection. Recently improved mass-spectrometry technology, however, may provide an ideal method for analysis of oligosaccharide chains.

Neuroblastomas (NBs) are common solid tumors in childhood and frequently occur in sympathetic ganglia and the adrenal medulla, both of which are derived from the neural crest. The clinical behavior of NBs is known to be varied. The NBs with favorable prognosis often differentiate to mature elements of sympathetic ganglia or regress spontaneously, whereas the NBs with unfavorable prognosis are resistant to chemotherapy, and their long-term outcome remains very poor despite the recent advance in the therapy for NBs. The outcome of NB patients is currently predicted on the basis of a set of risk factors, including age at diagnosis, advanced tumor stage, histological classification according to the international neuroblastoma pathology classification, *MYCN* amplification, DNA diploidy and chromosomal loss of 1p in tumors (4). Even when all of these markers are used in combination, it is sometimes difficult to correctly classify the aggressiveness of NBs, and additional markers that can be used as outcome predictors need to be discovered to establish a more effective therapeutic strategy (5).

Previous reports have described a link between expression of certain ganglioside molecules and the behavior of NBs, suggesting that expression of specific gangliosides by NBs may have diagnostic and prognostic potential (6-9). For example, NB cells express a higher level of GD2 than normal brain cells do (10). Characterization of ganglioside expression in the NBs of infants has revealed higher total pathway b ganglioside levels than in older children (8). By contrast, the unfavorable type of NB cells express lower levels of pathway b gangliosides, especially of GD1b, GT1b and GQ1b, than the non-progressive type of NB cells do (9). Based on the above evidence, we are focusing on ganglioside expression as a possible additional marker for predicting the outcome of NB.

In the present study we attempted to determine the overall profile of ganglioside expression in NB cell lines and in greater detail by using liquid chromatography in combination with mass-spectrometry (LC-MS) to determine levels of glycolipid expression. We then classified 11 NB cell lines into three groups based on their ganglioside expression profiles, especially their profiles of GD1a, GD2 and acetylated GD2 expression, and the classification was found to be correlated with the expression of neural-differentiation-related genes.

Materials and methods

Cell culture and antibodies (Abs). Eleven NB cell lines were used in this study. Nine of the cell lines, GOTO, NB1, NB9, NB16, NB69, IMR32, CHP126, CHP134 and KP-N-NS, were obtained from the Riken Cell Bank (Tsukuba, Ibaraki, Japan), and the other two cell lines, SK-N-SH and SK-N-RA, were a kind gift from Dr P. Reynolds. The characteristics of the cell lines are summarized in Table I. The *MYCN* gene is amplified in eight of these cell lines but not in the other three (NB69, SK-N-SH and SK-N-RA). The cells were cultured at 37°C in RPMI-1640 (Sigma-Aldrich Co, St. Louis, MO) supplemented with 10% FBS (Sigma) under a humidified atmosphere of 5% CO_2.

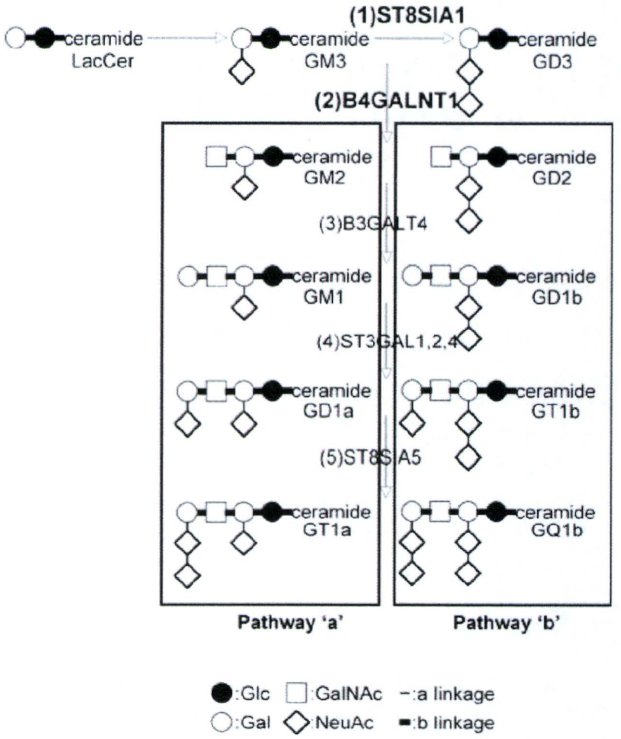

Figure 1. The pathways of ganglioside biosynthesis. The ganglioside biosynthesis pathways and glycosyltransferases that catalyze the synthesis of each ganglioside are shown. The glycosyltransferases whose mRNA expression level was investigated by RT-PCR in this study are indicated in bold type. 1: ST8SIA1, α2,8-sialyltransferase 1 (GD3 synthase); 2: B4GALNT1, β1,4-N-acetylgalactosaminyltransferase 1 (GM2/GD2 synthase); 3: B3GALT4, β1,3-galactosyltransferase 4 (GM1/GD1b synthase); 4: ST3GAL1,2,4, α2,3-sialyltansferase 1,2,4 (GD1a/GT1b synthase); 5: ST8SIA5, α2,8-sialyltransferase 5 (GT1a/GQ1b synthase).

A monoclonal Ab (mAb) specific for ganglioside GD2, 14.G2a, was purchased from Chemicon (Temecula, CA). Horseradish peroxidase (HRP)-conjugated rabbit anti-mouse immunoglobulin Ab was purchased from Dako (Glostrup, Denmark).

Lipid extraction. The lipids were extracted from the cell pellet with 2 ml of chloroform/methanol (2:1, v/v) and then with 2 ml of chloroform/isopropanol/water (7:11:2, v/v) in a sonicated bath. Total extracts were combined and evaporated to dryness. The lipids extracted from the cells were desalted by a SepPak C18 column (Waters, Milford, MA) and analyzed by HPTLC and LC-MS/MS as described below.

HPTLC analysis. TLC chemical staining and immunostaining were performed according to a previously described method (11). Briefly, the lipids were separated on plates

Table I. The summary of characteristics of the cell lines.

Cell line	Origin	Age (months)	Sex	Stage	MYCN[a]	Author/refs.
GOTO	Left adrenal gland	13	Male	IV	Amp	Sekiguchi *et al* (20)
NB1	Neck lymph node	33	Male	IV	Amp	Miyake *et al* (21)
NB9	Adrenal gland	22	Male	IV	Amp	Gilbert *et al* (22)
NB16	Bone marrow	35	Female	IV	Amp	Gilbert *et al* (22)
NB69	Adrenal gland	16	Male	III	Not amp	Gilbert *et al* (22)
IMR32	Abdomen	13	Male	IV	Amp	Tumilowicz *et al* (23)
CHP126	Retroperitoneum	14	Female	III	Amp	Schlesinger *et al* (24)
CHP134	Left adrenal gland	13	Male	IV	Amp	Schlesinger *et al* (24)
KP-N-NS	Brain	10	Female	IV	Amp	Yoshihara *et al* (25)
SK-N-SH	Bone marrow	48	Female	IV	Not amp	Biedler *et al* (26)
SK-N-RA[b]					Not amp	Helson, unpublished

[a]Amplification of MYCN.

precoated with Silica gel 60 (HPTLC sheets, Merck, Darmstadt Germany) by using a solvent system consisting of chloroform/methanol/water containing 0.2% $CaCl_2$ (5:4:1, v/v/v) in duplicate. The HPTLC plates were stained with resorcinol to detect the separated gangliosides. The ganglioside levels were quantitated after scanning the plates on a TLC scanner (model GS-930, Shimadzu). In parallel, other plates were dipped in a 0.1% polyisobutylmethacrylate (Sigma) cyclohexane solution for 1 min and blocked with 1% bovine serum albumin (BSA) in phosphate-buffered saline (PBS). The plates were incubated with the appropriate combination of primary Ab and HRP-conjugated secondary Ab, and then washed thoroughly. The Abs that bound to the plates were visualized with enhanced chemiluminescence reagent SuperSignal (Pierce, Rockford, IL) and detected by LAS-1000 (Fuji Film, Tokyo, Japan).

Acetylated GD2 (Ac-GD2) was detected as described previously (12). After chromatography, the O-acetyl groups were removed from the gangliosides by exposing the TLC plate to concentrated vapor of ammonium hydroxide in a closed chromatography tank for 12 h, and then allowing the plates to dry. The deacetylated chromatogram was immunostained with anti-GD2 Ab as described above.

LC/ESI-MS analysis. The extracted lipids were separated by high-performance LC (1200 series Capillary LC System, Agilent) equipped with a normal-phase column (Imtakt UK-silica, 150 x 0.3 mm). Chloroform/methanol/50 mM acetic acid-triethylamine in water (pH 4.2) = 83/16/1 (A) and methanol/50 mM acetic acid-triethylamine in water (pH 4.2) = 3/1 (B) were used as the solvents to determine the lipid composition. Elution was achieved with a linear gradient of 0-100% of B over 45 min at a flow rate of 3 µl/min. On-line MS and MS/MS were performed by using an Electrospray ionization (ESI)/ion trap (IT) type mass spectrometer (ESI-IT, Bruker Daltonics, Billerica, MA). The lipids were detected by the negative ion mode. The analytical conditions were set to 250°C for capillary temperature and m/z 150-2500 scan range.

Reverse transcription-PCR (RT-PCR) analysis. Total RNA was extracted from cells with an RNeasy Mini Kit (Qiagen, Valencia, CA), and cDNA was generated from 150 ng total RNA by using a FirstStrand cDNA Synthesis Kit (Pharmacia Biotech, Uppsala, Sweden). RT-PCR was performed by using a HotStarTaq Master Mix Kit (Qiagen) according to the manufacturer's protocol. The sets of primers used in this study are listed in Table II. The genes encode enzymes, those involved in gangliosides biosynthesis pathways indicated in Fig. 1, were examined for their expression. The products were separated on a 2% agarose gel and visualized by ethidium bromide staining.

Clustering analysis. The hierarchical clustering heat map was generated by using package R software (http://www.r-project.org/).

Results

Analysis of the composition of the gangliosides in NB cells by LC-MS. We established a condition of glycosphingolipid analysis by LC-MS that enables glycosphingolipid expression by cells to be determined. The lipids extracted from NB cells were separated by HPLC and analyzed by MS connected to HPLC on-line. All glycolipid species, the components considered to have ceramide backbones by LC-MS detection, were subjected to tandem mass spectrometry (MS/MS), and the molecular species was determined.

The extracted ion chromatogram (EIC) and the mass spectrum of the gangliosides extracted from the CHP134 cells are shown in Fig. 2 and Table III as an example of the results of an analysis. The EIC of the gangliosides and the acetylated gangliosides were superimposed in Fig. 2A and B, respectively. The expression levels of the gangliosides were quantified by calculating the areas of each peak on these chromatograms. Fig. 2C shows the MS/MS spectrum of the ion at m/z 1645.8 as a precursor and the structure of the molecular species characterized by the MS/MS fragment ions. The spectrum mainly consists of Y

Table II. The sets of primers used in this study.

Name of gene	Forward primer	Reverse primer
ST8SIA1	TGGGAAATGGTGGGATTCT	TGACAAAGGAGGGAGATTGC
B4GALNT1	GCTGCCTTAGAGCGTTAGACA	GCGAGCAGAAGGACCAGA
B3GALT4	AGGCAGGAACAGGACCTTCT	CCCATATCGCTGTCTTTAGTGAG
ST3GAL1	CAAATCCCGGAAACTCCAG	AGGAAGATGAAATCTGAAAATGGT
ST3GAL2	GTCCAGAGGTGGTGGATGAT	CAGCACCTCATTGGTGTTGT
ST3GAL4	GACCATCCTGAGTGATAAGAAGC	TTAGGATTGACATCCCAGATGA
ß-actin	CACCATGTACCCTGGCATT	GCCGATCCACACGGAGTA
NF-M	CAGGACCTCCTCAACGTCA	CACCCTCCAGGAGTTTTCTG
NF-H	CCGACATTGCCTCCTACC	GGCCATCTCCCACTTGGT
NCAM	AGTTTCTCTGCAGGTGGATATTG	GGCATCTCCTGCCACTTG
CHGA	GCGGTTTTGAAGATGAACTCTC	GCTCTTCCACCGCCTCTT
p75	GGATCTGATGCTCAAGATGGT	GTCTCTCTCTCTTCACTGGATGG
Phox2a	CACTACCCCGACATTTACACG	GCTCCTGTTTGCGGAACTT
Phox2b	CTACCCCGACATCTACACTCG	CCTGCTTGCGAAACTTGG
MYCN	CCACAAGGCCCTCAGTACC	CCTCTTCATCATCTTCATCATCTG
p73	ACGTTTGAGCACCTCTGGA	CGCCCACCACCTCATTATT
TrkA	AGGAAGGCCATTCTCTGCTAC	GGCTGAAGTCTTTGGAGAGC
TrkB	GGGACGTGTACAGCACTGACT	CCTGTACATGATGCTCTCTGGA
TrkC	TCTGGGAGATCTTCACCTATGG	CTTGGGTAATGCACTCAATGAC
N-cadherin	CCTGAAGCCAACCTTAACTGA	TGGAGGGATGACCCAGTCT
PTN	AACTGACCAAGCCCAAACCT	GGTGACATCTTTTAATCCAGCA

Table III. Fragment ions detected by LC-MS/MS spectra of endogenous GSLs from CHP134 cells.

Parent (m/z)	Fragments
GM3 (1152.2, $[M-H]^-$)	1133.6, 860.5, 698.4, 680.4, 536.4, 518.4
GM2 (1355.5, $[M-H]^-$)	1339.4, 1156.6, 1063.6, 860.5, 698.5, 680.4, 536.5
GM1 (1517.2, $[M-H]^-$)	1498.5, 1456.6, 1438.6, 1225.6, 1063.6, 1045.6, 860.6, 698.5, 680.4, 536.5
GD1a (903.9, $[M-2H]^{2-}$)	1516.6, 1498.6, 1225.5, 1151.4, 1063..5, 997.5, 860.5, 680.4, 536.6, 290.0
GT1a (1049.6, $[M-2H]^{2-}$)	1810.4, 1516.5, 1226.4, 903.2, 581.1, 537.2
GD3 (721.4, $[M-2H]^{2-}$)	1151.5, 1133..6, 860.5, 698.5, 581.1, 537.4, 290.0
GD2 (822.9, $[M-2H]^{2-}$)	1354.6, 1337.6, 1063.6, 860.5, 698.5, 680.4, 581.1, 536.4, 290.0
GD1b (904.0, $[M-2H]^{2-}$)	1516.6, 1498.6, 1225.6, 1064.6, 1046.4, 997.5, 860.5, 698.5, 680.4, 581.1, 536.5, 290.0
GT1b (1049.6, $[M-2H]^{2-}$)	1807.5, 1789.4, 1516.7, 1499.6, 1225.5, 1064.666, 903.8, 860.6, 680.4, 581.1, 537.2, 290.1
AcGD1a (925, $[M-2H]^{2-}$)	1558.4, 1516.6, 1225.6, 1151.8, 1064.7, 860.6, 698.4, 680.0, 536.4, 332.2, 290.0
Ac-GD3 (743.0, $[M-2H]^{2-}$)	1151.5, 860.5, 698.4, 680.4, 623.2, 536.5, 332.0, 290.0
Ac-GD2 (843.9, $[M-2H]^{2-}$)	1354.6, 1063.6, 860.5, 698.5, 680.4, 623.1, 536.5, 332.2, 290.0
Ac-GD1b (925.1, $[M-2H]^{2-}$)	1516.5, 1225.6, 1063.5, 1045.6, 860.5, 698.5, 623.1, 536.5, 332.1, 290.0
Ac-GT1b (1070.6, $[M-2H]^{2-}$)	1516.5, 1048.2, 623.6
A (758.4, $[M-2H]^{2-}$)	1225.5, 1063.4, 860.4, 698.4, 536.5, 290.1
B (860.0, $[M-2H]^{2-}$)	1428.5, 1063.6, 1038.2, 997.4, 876.1, 698.6, 673.1, 536.4, 289.9
C (940.8, $[M-2H]^{2-}$)	1590.5, 1429.6, 1411.6, 1225.5, 1063.5, 860.6, 698.6, 536.4, 290.0

ions, i.e., the Y3α at m/z 1354.6 (loss of outer sialic acid), Y2α at m/z 1063.6 (loss of inner sialic acid), Y2α/Y2ß at m/z 860.5 (loss of outer GalNAc), Y1 at m/z 698.5 (Lac-Cer) and Y0 at m/z 536.5 [Cer, the sphingosine (d18:1) with

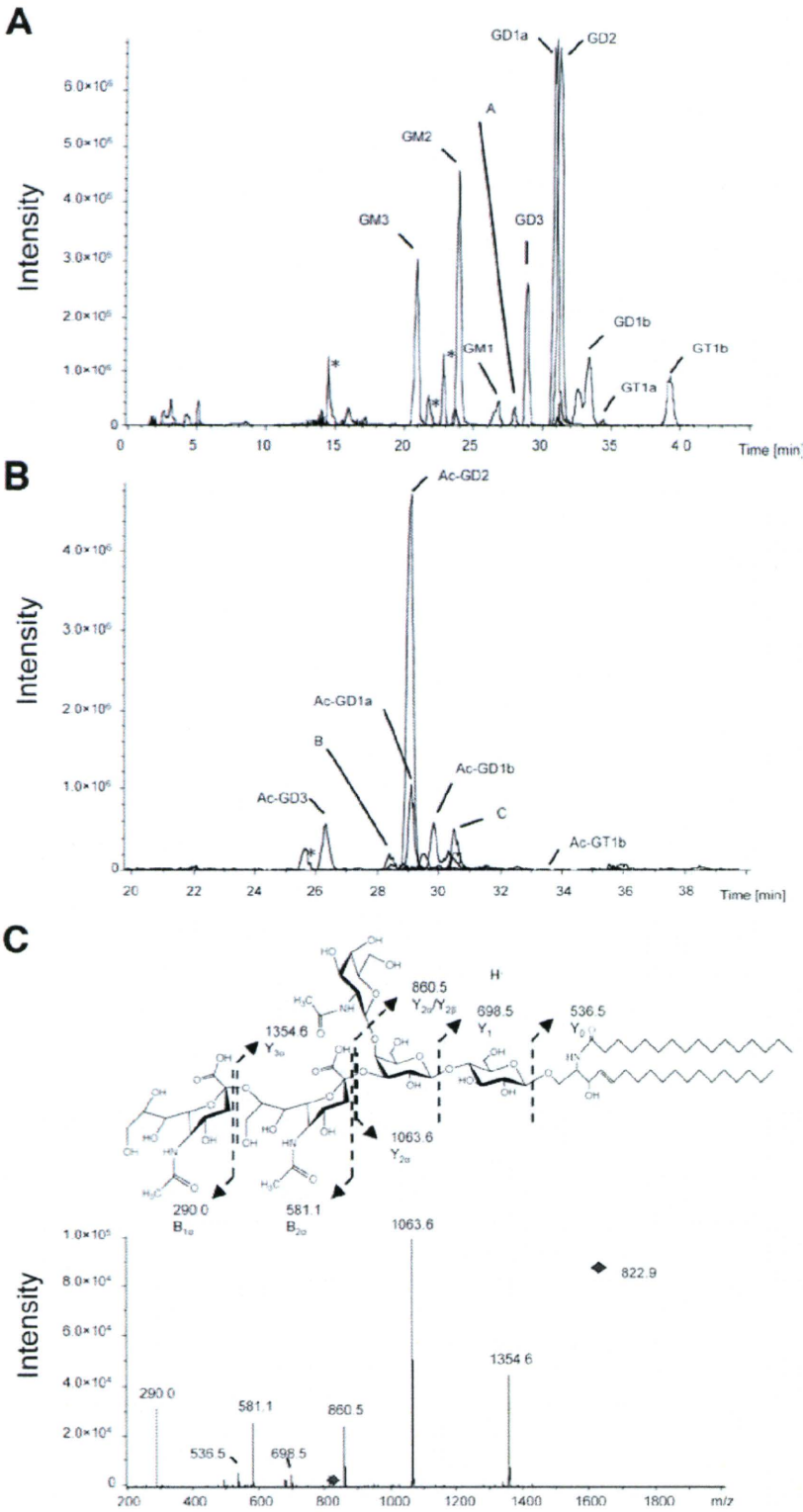

Figure 2. The LC-MS analysis of gangliosides extracted from the CHP134 cells. (A) Superimposed EIC of GM3, GM2, GM1, peak A, GD3, GD1a, GD2, GD1b, GT1a and GT1b extracted from $2x10^6$ of CHP134 cells. (B) Superimposed EIC of Ac-GD3, peak B, Ac-GD1a, Ac-GD2, Ac-GD1b, peak C and Ac-GT1b extracted from $2x10^6$ of CHP134 cells. Asterisks indicate the impurity peak that did not represent molecular species of ceramide. (C) The MS/MS spectrum of the ion at m/z 822.9 $[M-2H]^{2-}$ as a precursor and the chemical structure of the molecular species characterized by the MS/MS fragment ions. All fragment ions appeared as singly charged species.

C16:0 fatty acid] (Fig. 2C). Two B ions, i.e., B1α at m/z 290.0 (Neu5Ac) and B2α at m/z 581.1 (Neu5Ac-Neu5Ac), were also detected (Fig. 2C). Since these fragment patterns corresponded to those of standard GD2 (data not shown), the

Table IV. Ganglioside composition of human neuroblastoma cell lines (Cer: d 18:1/16:0).

	% of total gangliosides										
	SK-N-SH	SK-N-RA	NB69	GOTO	NB9	CHP134	KP-N-NS	IMR32	NB1	NB16	CHP126
GM3	44.44	17.04	11.05	13.02	6.43	7.28	4.00	11.50	13.19	18.11	4.96
GM2	9.93	8.63	22.19	31.77	21.55	11.51	11.34	31.31	23.41	17.75	20.54
GM1	9.72	11.04	12.86	4.43	4.80	8.22	6.56	5.52	4.63	8.30	4.20
GD1a	29.13	33.38	23.30	33.53	53.29	19.31	21.14	7.62	5.20	7.01	8.40
GT1a	0.00	0.00	0.00	0.00	0.00	0.15	0.27	0.00	0.00	0.00	0.00
GD3	0.48	13.23	1.35	2.05	2.71	6.17	3.99	3.67	4.61	4.23	3.75
GD2	0.10	3.97	4.25	7.59	3.77	21.43	23.94	21.88	26.60	25.99	37.11
GD1b	0.47	5.38	7.29	0.00	0.00	6.21	12.89	0.45	0.62	2.25	7.36
GT1b	0.04	1.52	0.10	0.14	0.51	2.94	3.40	0.12	0.09	0.45	0.93
AcGD1a	0.52	0.61	0.56	1.30	1.77	1.46	1.61	0.28	0.28	0.42	0.33
AcGD3	0.00	0.71	0.00	0.07	0.00	1.15	0.00	0.33	1.24	0.26	0.28
AcGD2	0.00	0.77	0.66	1.48	0.65	7.83	7.71	9.17	13.78	12.07	9.17
AcGD1b	0.00	0.00	0.00	0.00	1.02	1.53	1.35	0.41	0.45	0.81	0.83
AcGT1b	0.00	0.00	0.00	0.00	0.00	0.03	0.00	0.00	0.00	0.00	0.00
A	0.00	0.00	5.95	0.99	0.41	3.87	0.51	1.84	2.04	0.00	0.00
B	3.09	0.53	1.93	0.22	0.49	0.00	0.62	0.70	0.34	0.77	1.46
C	2.08	3.18	8.49	3.40	2.60	0.93	0.65	5.20	3.53	1.57	0.69

A, NeuAc-Hex+HexNAc+LacCer; B, NeuAc+HexNAc+(Gal-GlcNAc)+LacCer; C, NeuAc+$(Gal\text{-}GlcNAc)_2$+LacCer.

structure of the ion at m/z 822.9 $[M\text{-}2H]^{2-}$ was identified as that of GD2.

Fragment ions observed by LC-MS/MS spectra of each peak in Fig. 2A and B and the deduced molecular species were listed in Table III. The sugar composition of peak A, B and C did not correspond to ganglio-series gangliosides, and the structure was predicted as NeuAc-Hex+HexNAc+LacCer, NeuAc+HexNAc+Hex-HexNAc+LacCer and NeuAc+$(Hex\text{-}HexNAc)_2$+LacCer, respectively.

The composition of the individual gangliosides in each cell line was expressed as a percentage of its peak area to the total area of all of the ganglioside peaks. Since each ganglioside carried at least two major ceramides, d 18:1/16:0 and d 18:1/24:1, a semi-quantitative value of each ganglioside was calculated for each major ceramide having m/z 535.6 and 646.6, and the values are summarized in Table IV (d 18:1/16:0) and Table V (d 18:1/24:1). It should be noted that several gangliosides also carried a few minor ceramide species (d 18:1/18:0, d 18:1/20:0, d 18:1/22:0) (data not shown).

As shown in Tables IV and V, expression of GD1a, one of the pathway a ganglioside, was high in SK-N-SH, SK-N-RA, NB69, GOTO, NB9, CHP134 and KP-N-NS cells and low in IMR32, NB1, NB16 and CHP126 cells, whereas expression of GD2, a pathway b ganglioside, was high in CHP134, KP-N-NS, IMR32, NB1, NB16 and CHP126 cells and low in SK-N-SH, SK-N-RA, NB69, GOTO and NB9 cells.

Interestingly, the gangliosides containing an O-acetylated sialic acid were detected in all of the NB cell lines (Tables IV and V). Acetylation was observed in GD1a, GD3, GD2, GD1b and GT1b, but the proportion of the acetylated-gangliosides varied from cell line to cell line. Expression of Ac-GD2 was high in CHP134, KP-N-NS, IMR32, NB1, NB16 and CHP126 cells, accounting for >10% of all gangliosides in NB1 and NB16 cells, and low in SK-N-SH, SK-N-RA, NB69, GOTO and NB9 cells (Tables IV and V).

Analysis of ganglioside composition by HPTLC. To confirm the reliability of the profiles of ganglioside expression in NB cells obtained by LC-MS, samples of the same lipid extract preparations were analyzed by HPTLC, and the relative amounts of the individual gangliosides they contained were determined by densitometry (Fig. 3, Table VI). Nine bands stained with resorcinol were tentatively assigned to GM3, GM2, GM1, GD3, GD2, GD1a, GD1b, GT1a and GT1b, respectively, by comparing the Rf values with ganglioside standards. All of them were also detected by LC-MS and the expression profiles of these gangliosides were highly consistent with those detected by LC-MS. However, the other gangliosides, including acetylated forms, that were identified by LC-MS were not detected by HPTLC. For example, HPTLC could not detect GD2 in SK-N-SH, SK-N-RA, NB69, GOTO and NB9, although its expression in the cells was detected by LC-MS.

GD2 and Ac-GD2 ganglioside detected by TLC immunostaining. We performed a TLC immunostaining analysis to confirm the differences in the level of GD2 expression among the NB cell lines. As shown in Fig. 4A, the lipid extracts from SK-N-SH, SK-N-RA, NB69, GOTO and NB9 cells were weakly or hardly stained with anti-GD2 mAb 14.G2a (lanes 1-5), whereas those of CHP-134, KP-N-NS, IMR32,

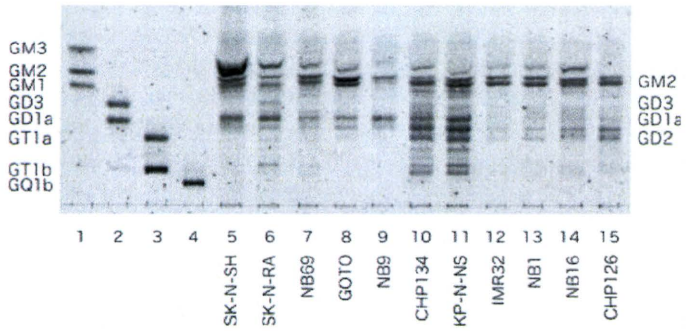

Figure 3. High-performance thin-layer chromatogram of gangliosides extracted from the human neuroblastoma cell lines. Lipids extracted from $1x10^7$ cells were separated on an HPTLC plate and visualized by resorcinol spraying. GM3, GM2, GM1, GD3, GD1a, GT1a, GT1b and GQ1b were used as ganglioside standards (lanes 1-4).

Table V. Ganglioside composition of human neuroblastoma cell lines Cer: d 18:1/24:1.

	% of total gangliosides										
	SK-N-SH	SK-N-RA	NB69	GOTO	NB9	CHP134	KP-N-NS	IMR32	NB1	NB16	CHP126
GM3	36.89	6.22	3.41	4.90	4.80	1.20	0.49	3.05	4.88	7.88	0.60
GM2	8.40	17.05	28.82	15.26	5.93	6.79	8.08	24.80	19.21	12.06	15.25
GM1	7.11	13.94	4.6	7.24	9.65	6.86	5.43	5.19	3.6	6.52	2.44
GD1a	37.09	40.36	45.55	57.80	35.00	29.28	26.75	14.56	8.48	11.58	13.64
GT1a	0.00	0.00	0.00	0.13	0.00	0.25	0.54	0.00	0.00	0.00	0.34
GD3	0.00	1.34	0.79	0.83	20.53	8.10	3.92	3.53	4.89	4.70	2.62
GD2	0.00	2.28	6.70	2.37	3.83	13.05	10.14	25.34	27.55	27.02	40.60
GD1b	1.66	0.00	0.00	0.00	7.11	6.96	19.07	0.89	2.03	3.27	0.00
GT1b	0.00	0.20	0.18	0.87	2.20	3.00	3.35	0.00	0.00	0.61	2.08
AcGD1a	3.04	1.29	3.04	4.56	1.26	2.46	2.61	0.70	0.50	0.74	1.01
AcGD3	0.00	0.00	0.00	0.00	0.00	1.07	0.00	0.31	0.97	0.81	0.00
AcGD2	0.00	0.58	2.64	1.04	1.10	11.07	10.71	14.15	21.59	20.25	16.42
AcGD1b	0.00	0.00	0.00	0.78	3.68	3.19	6.81	0.00	0.92	1.75	2.54
AcGT1b	0.15	0.00	0.00	0.00	0.14	1.68	0.00	0.00	0.00	0.00	0.00
A	0.00	6.19	1.22	0.94	0.00	3.12	0.53	1.64	1.55	0.00	0.00
B	3.97	2.68	0.00	0.79	1.38	0.67	0.82	1.04	0.57	0.77	1.70
C	1.67	7.88	3.04	2.48	3.38	1.26	0.77	4.81	3.27	2.05	0.74

A, [NeuAc-Hex+HexNAc+LacCer; B, [NeuAc+HexNAc+(Gal-GlcNAc)+LacCer; C, [NeuAc+$(Gal-GlcNAc)_2$+LacCer.

Table VI. Ganglioside composition of human neuroblastoma cell lines (HPTLC).

	% of total gangliosides										
	SK-N-SH	SK-N-RA	NB69	GOTO	NB9	CHP134	KP-N-NS	IMR32	NB1	NB16	CHP126
GM3	52.45	20.65	17.56	15.01	7.34	5.92	3.40	11.66	14.09	17.40	7.18
GM2	25.36	29.50	49.09	59.76	42.39	18.83	19.27	63.44	49.54	35.99	34.89
GM1	1.68	1.12	4.84	1.98	0.51	7.81	8.87	2.99	3.80	4.31	5.24
GD1a	20.50	29.27	19.86	20.51	49.75	16.06	13.97		2.17	6.60	0.48
GT1a		2.54	0.28	0.60		6.70	8.85				
GD3		9.26	6.35	2.13		5.86	5.30	10.40	15.08	9.81	11.91
GD2						15.86	15.21	11.52	15.33	21.86	34.22
GD1b						12.18	11.92			0.56	2.04
GT1b		7.66	2.03			10.78	13.22			3.47	4.05

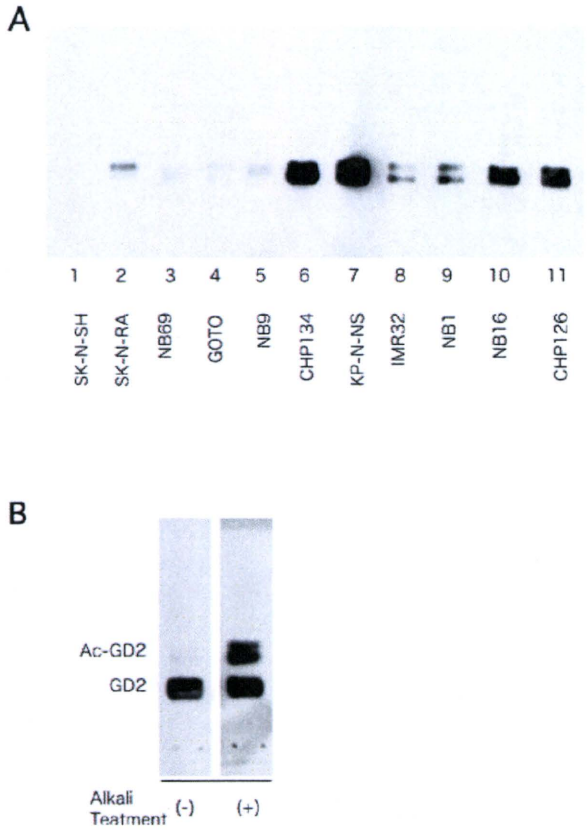

Figure 4. TLC immunostaining of ganglioside GD2 and Ac-GD2. (A) The lipids extracted from $1x10^5$ cells were separated on HPTLC plates and immunostained with mAb 14.G2a. (B) The lipids of $1x10^5$ CHP134 cells separated on an HPTCL plate was treated with alkali and immunostained with mAb 14.G2a.

NB1, NB16 and CHP126, were strongly or significantly stained (lanes 6-11). These results are essentially consistent with those obtained with LC-MS.

As shown in Fig. 4B, when the TLC plate was treated with alkali after TLC development to remove acetyl group from sialic acid residues, the band newly produced by the conversion of Ac-GD2 to GD2 was detected at a position with a higher Rf value than GD2. Taken together with the results of the LC-MS analysis, these findings show that Ac-GD2 is expressed in NB cells.

Clustering analysis of gangliosides expressed in NB cells. The above results imply that the NB cell lines have distinct glycolipid expression profiles that allow them to be classified in several groups. As shown in Tables IV, V and Fig. 5, the profiles of glycosphingolipid GD1a, GD2 and acetylated GD2 expression varied from cell line to cell line. We therefore performed a clustering analysis centered on these three glycosphingolipids, and the results showed that the NB cell lines could be classified into three groups based on their expression of these three gangliosides (Fig. 5B). The NB9, NB69, SK-N-SH, SK-N-RA and GOTO cells were characterized by high expression of GD1a and low expression of GD2/acetylated GD2 and classified as type A here, whereas CHP126, IMR32, NB1 and NB16 cells were characterized by low expression of GD1a and high expression of GD2/acetylated GD2 and classified as type B. CHP134 and KP-N-NS cells, on the other hand, were characterized by expression of both GD1a and GD2/acetylated GD2 and classified as type AB. Interestingly, all three *MYCN* non-amplified cell lines were classified as type A.

Expression of ganglioside synthase mRNA detected by RT-PCR in NB cell lines. To investigate the relationship between ganglioside expression and the level of expression of enzymes involved in ganglioside biosynthesis, RT-PCR analysis was used to investigate the NB cell lines for mRNA expression of two ganglioside synthases. As shown in Fig. 6A, the results showed a high level of GD3 synthase mRNA expression (ST8SIA1) (Fig. 1) in the types B and AB cell lines, whereas mRNA expression of B4GALNT1, which is responsible for catalyzing the synthesis of both GM2 and GD2 (Fig. 1), was detected in all of the cell lines.

RNA expression of neural differentiation markers detected by RT-PCR in NB cell lines. To investigate the biological significance of the classification of NB cell lines based on their ganglioside expression profile, we investigated expression of neural-differentiation-related genes by RT-PCR and assessed the relation between their expression and glycolipid expression. As shown in Fig. 6B and C, RT-PCR analysis revealed that mRNA expression of the neural-differentiation-related genes *Phox2a* and *b*, *TrkC*, neurofilament, and *N-CAM* was positively correlated with GD2 and acetylated GD2 expression in the NB cell lines. By contrast, mRNA expression of pleiotrophin (*PTN*) tended to be high in cell lines with a low level of GD2 expression. All *MYCN* non-amplified cells show low *MYCN* expression by RT-PCR (Fig. 6D).

Discussion

In this study we used an LC-MS analysis system to detect glycosphingolipid expression in NB cells and clearly demonstrated its great potential as a tool for glycosphingolipid research. As shown above, the LC-MS analysis was highly sensitive and enabled detection of a number of glycolipids expressed in NB cells that were not detected by HPTLC analysis. This approach allows determination of even low percentages of lipids of each molecular species and showed clear differences between the glycosphingolipid profiles of a series of NB cell lines. The method described in this report should be useful and easily adaptable to glycosphingolipid analysis of various types of tumor cells.

In this study we also demonstrated the presence of acetylated forms of gangliosides in NB cells. As described above, we detected acetylated forms of GD1a, GD3, GD2, GD1b and GT1b in NB cells by LC-MS analysis and expression of acetylated GD2 was found to be high. For example, Ac-GD2 accounted for >10% of the total ganglioside in NB1 and NB16 cells. The presence of acetylated GD2 was correlated with expression of GD2. Ye and Cheung demonstrated that O-acetylated GD2 is a naturally occurring ganglioside derivative in human tumors, including in NB, by using mAb 3F8, which specifically recognizes GD213, and our data are consistent with their findings.

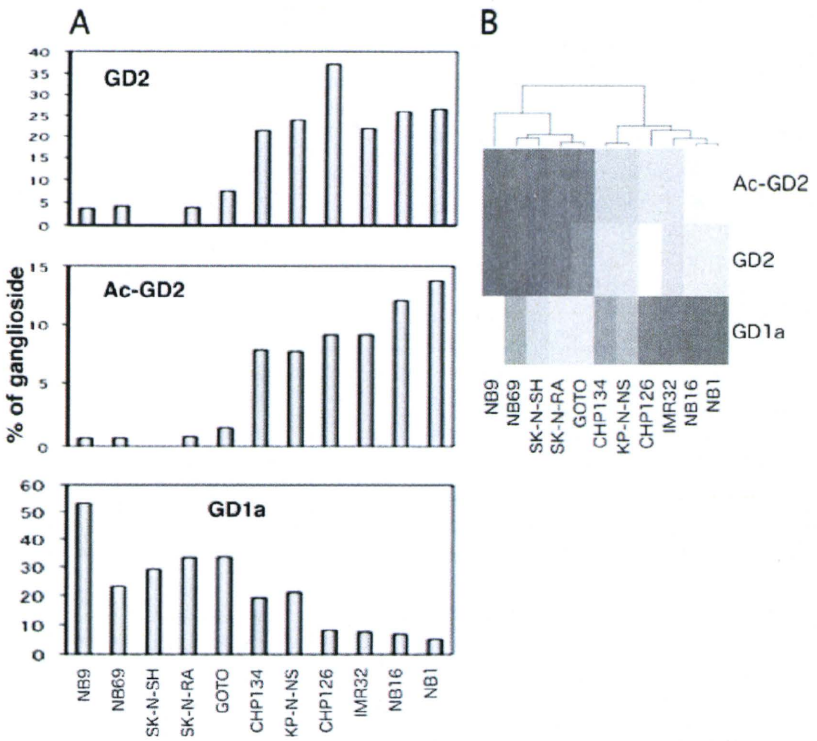

Figure 5. Hierarchical clustering of differentially expressed gangliosides. (A) The percentage of Ac-GD2, GD2 and GD1a to the total gangliosides of NB cell lines. (B) The clustering tree shows the expression pattern and similarity in cell lines. The strength of the gangioside expression was gradually increased on the heat map.

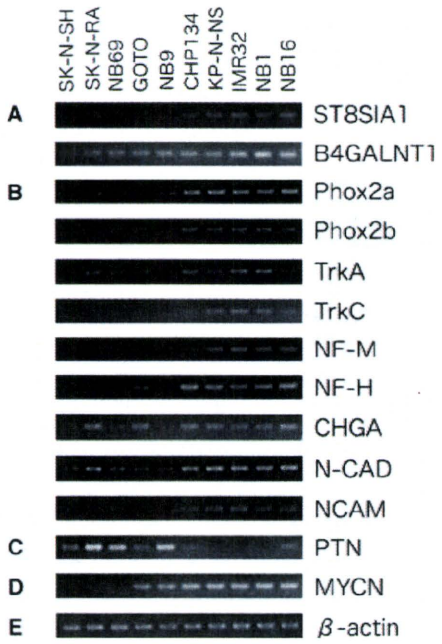

Figure 6. Analysis of expression of neural-differentiation-related genes and glycosyltransferase genes by RT-PCR. (A) Glycosyltransferase genes (Fig. 1), (B) *Phox2a*, paired-like (aristaless) homeobox 2a; *Phox2b*, paired-like homeobox 2b; *TrkA*, neurotrophic tyrosine kinase, receptor, type 1, also known as *NTRK1*; *TrkC*, neurotrophic tyrosine kinase, receptor, type 3, also known as *NTRK3*; *NF-M*, neurofilament 160 kDa subunit; *NF-H*, neurofilament 200 kDa subunit; *CHGA*, chromogranin A; *N-CAD*, N-cadherin and *NCAM*, neural cell adhesion molecule, (C) *PTN*, pleiotrophin, (D) *MYCN*, v-myc myelocytomatosis viral related oncogene, (E) ß-actin was used as an internal control.

The biological significance of ganglioside acetylation has not been fully elucidated, but it is thought to modulate cell function by regulating the ability of gangliosides to bind cell adhesion molecules. For example, CD22ß (also called Siglec-2) is a B-cell-restricted phosphoprotein that mediates interactions with other cells via binding with α2-6-linked sialic acids on glycoconjugates, and the fact that the binding can be inhibited by 9-O-acetylation of sialic acids suggests that CD22ß adhesion events are regulated by ganglioside acetylation (14,15). In childhood acute lymphoblastic leukemia, on the other hand, administration of exogenous GD3 induces apoptosis, whereas O-acetylated GD3 fails to induce similar effects, suggesting that O-acetylation of GD3 promotes leukemia cell survival by preventing apoptosis (16,17). Although the significance of acetylated GD2 in NB cells still remains largely unknown, further investigation should shed light on the functional role of gangliosides in the biological behavior of NB cells.

The NB cell lines were classified into three types based on their of ganglioside expression profiles determined by LC-MS analysis, namely, type A, with a high level of expression of GD1a but low level or no expression of GD2/acetylated GD2, and consisting of SK-N-SH, SK-N-RA, NB69, GOTO and NB9 cells, type B, with a high level of expression of GD2/acetylated GD2 but low level or no expression of GD1a, and consisting of IMR32, NB1, NB16 and CHP126 cells, and type AB, which express both GD1a and GD2/acetylated GD2, and consisting of CHP134 and KP-N-NS cells. The results of the RT-PCR analyses indicated that the ganglioside expression profiles of NBs correlated with their ganglioside

synthase expression pattern. As shown in Fig. 6, ST8sia1, which catalyzes the synthesis of GD3 from GM3, was expressed only in the types B and AB NB cell lines and not in any of the type A NB cell lines, whereas B4galnt1, which catalyzes the synthesis of both GM2 and GD2, was expressed in all the NB cell lines tested in this study.

Expression of GD2 ganglioside is characteristic of cells of neuroectodermal origin, and a high level of expression has been reported in NB cells, whereas the GD2 distribution in humans is limited to neurons and peripheral nerve fibers (18). Thus, GD2 appears to be useful as a target for the treatment of NB. However, our findings in this study indicated that the level of GD2 expression in NB cells is variable and that NB cells can be classified based on their pattern of expression of ganglio-series gangliosides, including GD2. Since increased shedding of GD2 ganglioside and *MYCN* amplification jointly characterize the aggressive type of NB cells (19), classification of NBs based on their ganglioside expression profile may have prognostic value. Our observation that the ganglioside expression profiles are closely related to the expression of neural-differentiation-related genes appears to further support this notion.

In conclusion, we have demonstrated the usefulness of the LC-MS analysis system as a tool for glycosphingolipid research. Eighteen species of glycosphingolipids containing gangliosides of a and b pathways and their acetylated forms were detected. The expression ratios of the glycosphingolipids were determined, and were compared among 11 of NB cell lines. Based on the results, it was indicated that these NB cell lines could be classified into three categories. Although more detailed experiments are clearly needed, further investigations using the new method should provide a new approach to determining the biological significance of glycosphingolipids in NBs and identifying novel biomarkers for predicting the outcome of NB.

Acknowledgments

We are grateful to Dr P. Reynolds for providing the SK-N-SH and SK-N-RA cells. We thank Ms. H. Kiyokawa for her assistance to prepare the manuscript. This work was supported by a grant from the Japan Health Sciences Foundation for Research on Publicly Essential Drugs and Medical Devices (KHA1004), Health and Labour Sciences Research Grants (Research on Human Genome Tailor made and Research on Publicly Essential Drugs and Medical Devices H18-005, the 3rd-term Comprehensive 10-year strategy for Cancer Control H19-010), a Grant for Child Health and Development from the Ministry of Health, Labour and Welfare of Japan, and by CREST, JST. This work was supported in part by the Grant-in-Aid for Cancer Research (16-16) from the Ministry of Health, Labor and Welfare.

References

1. Ledeen RW and Yu RK: Gangliosides: structure, isolation, and analysis. Methods Enzymol 83: 139-191, 1982.
2. Van Echten G and Sandhoff K: Ganglioside metabolism. Enzymology, topology, and regulation. J Biol Chem 268: 5341-5344, 1993.
3. Hakomori S: Tumor malignancy defined by aberrant glycosylation and sphingo(glyco)lipid metabolism. Cancer Res 56: 5309-5318, 1996.
4. Weinstein JL, Katzenstein HM and Cohn SL: Advances in the diagnosis and treatment of neuroblastoma. Oncologist 8: 278-292, 2003.
5. Ohira M, Oba S, Nakamura Y, Hirata T, Ishii S and Nakagawara A: A review of DNA microarray analysis of human neuroblastomas. Cancer Lett 228: 5-11, 2005.
6. Schengrund CL, Repman MA and Shochat SJ: Ganglioside composition of human neuroblastomas. Correlation with prognosis. A Pediatric Oncology Group Study. Cancer 56: 2640-2646, 1985.
7. Schengrund CL and Shochat SJ: Gangliosides in neuroblastomas. Neurochem Pathol 8: 189-202, 1988.
8. Kaucic K, Etue N, LaFleur B, Woods W and Ladisch S: Neuroblastomas of infancy exhibit a characteristic ganglioside pattern. Cancer 91: 785-793, 2001.
9. Hettmer S, Malott C, Woods W, Ladisch S and Kaucic K: Biological stratification of human neuroblastoma by complex B pathway ganglioside expression. Cancer Res 63: 7270-7276, 2003.
10. Wu ZL, Schwartz E, Seeger R and Ladisch S: Expression of GD2 ganglioside by untreated primary human neuroblastomas. Cancer Res 46: 440-443, 1986.
11. Nakamura K, Suzuki M, Taya C, Inagaki F, Yamakawa T and Suzuki A: A sialidase-susceptible ganglioside, IV3 alpha (NeuGc alpha 2-8NeuGc)-Gg4Cer, is a major disialoganglioside in WHT/Ht mouse thymoma and thymocytes. J Biochem 110: 832-841, 1991.
12. Kushi Y, Ogura K, Rokukawa C and Handa S: Blood group A-active glycosphingolipids analysis by the combination of TLC-immunostaining assay and TLC/SIMS mass spectrometry. J Biochem 107: 685-688, 1990.
13. Ye JN and Cheung NK: A novel O-acetylated ganglioside detected by anti-GD2 monoclonal antibodies. Int J Cancer 50: 197-201, 1992.
14. Sjoberg ER, Powell LD, Klein A and Varki A: Natural ligands of the B cell adhesion molecule CD22 beta can be masked by 9-O-acetylation of sialic acids. J Cell Biol 126: 549-562, 1994.
15. Kelm S, Schauer R, Manuguerra JC, Gross HJ and Crocker PR: Modifications of cell surface sialic acids modulate cell adhesion mediated by sialoadhesin and CD22. Glycoconj J 11: 576-585, 1994.
16. Malisan F, Franchi L, Tomassini B, *et al*: Acetylation suppresses the proapoptotic activity of GD3 ganglioside. J Exp Med 196: 1535-1541, 2002.
17. Mukherjee K, Chava AK, Mandal C, Dey SN, Kniep B, Chandra S and Mandal C: O-acetylation of GD3 prevents its apoptotic effect and promotes survival of lymphoblasts in childhood acute lymphoblastic leukaemia. J Cell Biochem 105: 724-734, 2008.
18. Varki A: Glycosylation changes in cancer. In: Essentials of Glycobiology. Varki A and Cummings R (eds). Cold Spring Harbor Laboratory Press, New York, 1999.
19. Valentino L, Moss T, Olson E, Wang HJ, Elashoff R and Ladisch S: Shed tumor gangliosides and progression of human neuroblastoma. Blood 75: 1564-1567, 1990.
20. Sekiguchi M, Oota T, Sakakibara K, Inui N and Fujii G: Establishment and characterization of a human neuroblastoma cell line in tissue culture. Jpn J Exp Med 49: 67-83, 1979.
21. Miyake S, Shimo T, Kitamura Y, Nojyo T, Nakamura S, Imashuku S and Abe T: Characteristics of continuous and functional cell line NB-1, derived from a human neuroblastoma. Autonomic Nervous System 10: 115-120, 1973.
22. Gilbert F, Balaban G, Moorhead P, Bianchi D and Schlesinger H: Abnormalities of chromosome 1p in human neuroblastoma tumors and cell lines. Cancer Genet Cytogenet 7: 33-42, 1982.
23. Tumilowicz JJ, Nichols WW, Cholon JJ and Greene AE: Definition of a continuous human cell line derived from neuroblastoma. Cancer Res 30: 2110-2118, 1970.
24. Schlesinger HR, Gerson JM, Moorhead PS, Maguire H and Hummeler K: Establishment and characterization of human neuroblastoma cell lines. Cancer Res 36: 3094-3100, 1976.
25. Yoshihara T, Ikushima S, Hibi S, Misawa S and Imashuku S: Establishment and characterization of a human neuroblastoma cell line derived from a brain metastatic lesion. Hum Cell 6: 210-217, 1993.
26. Biedler JL, Helson L and Spengler BA: Morphology and growth, tumorigenicity, and cytogenetics of human neuroblastoma cells in continuous culture. Cancer Res 33: 2643-2652, 1973.

Cytometry Research 20(2):27～33, 2010

原 著

9 colorフローサイトメトリーによる小児白血病のマーカー解析

清河 信敬[1,2], 恩田 恵子[1,2,3], 高野 邦彦[4], 藤本 純一郎[1,2], 真部 淳[2,5], 康 勝好[2,6], 小原 明[2,7], 林 泰秀[2,8], 花田 良二[2,6], 土田 昌宏[2,9]

Immunocytological diagnosis of pediatric leukemia using 9-color flow cytometry

Nobutaka Kiyokawa M.D., Ph.D.[1,2], Keiko Onda M.D., Ph.D.[1,2,3], Kunihiko Takano C.C.[4], Junichiro Fujimoto M.D., Ph.D.[1,2], Atsushi Manabe M.D., Ph.D.[2,5], Katsuyoshi Ko M.D., Ph.D.[2,6], Akira Ohara M.D., Ph.D.[2,7], Yasuhide Hayashi M.D., Ph.D.[2,8], Ryoji Hanada M.D., Ph.D.[2,6], Masahiro Tsuchida M.D., Ph.D.[2,9]

[1] Department of Pediatric Hematology and Oncology Research, National Research Institute for Child Health and Development
[2] Tokyo Children's Cancer Study Group
[3] Department of Pediatrics, Juntendo University School of Medicine
[4] Beckman Coulter
[5] Department of Pediatrics, St. Luke's International Hospital
[6] Department of Hematology and Oncology, Saitama Children's Medical Center
[7] Department of Pediatrics, Toho University Omori Medical Center
[8] Gunma Children's Medical Center
[9] Ibaraki Children's Hospital

Abstract

Aim. We are in charge of the central diagnosis and cell preservation as a part of childhood acute lymphoblastic leukemia treatment study in Tokyo children's cancer study group. It is necessary to diagnose with a minimal quantity of specimen, to preserve leukemic cells effectively as possible. On the other hand, recent progress in multi-color flow cytometry enable to analyze cell marker of leukemia in more detail. We therefore we intended to perform a immuno-phenotypic diagnosis of childhood acute lymphoblastic leukemia by nine-color analysis with digital flow cytometer.

Methods. We examined cell markers of childhood acute lymphoblastic leukemia cells by nine-color analysis using digital flow cytometers. We decided the combination of the monoclonal antibodies for nine color analysis based on the recommendation of Japan Pediatric Leukemia/Lymphoma Study Group using commercially available fluorescence-laveled antibodies.

Results. Nine colors that we used in this study were fluorescein isothyocyanate, phycoerythrin (PE), phycoerythrin-Texas Red, Peridinin Chlorophyll Protein - cyanin (Cy) 5.5, PE-Cy7, allophycocyanin (APC), APC-Cy7, Pacific Blue, and Cascade Yellow. Using list mode compensation, nine color marker analysis of childhood leukemia was easy to perform.

Discussion. Although several problems need to be solved are present, nine-color analysis using digital flow cytometer is useful to obtain precise information of antigen expression as well as save precious specimen of childhood acute lymphoblastic leukemia.

Key words : Flow cytometry ; multi-color analysis ; childhood acute lymphoblastic leukemia.

【はじめに】

東京小児がん研究グループ（Tokyo Children Cancer Study Group, TCCSG）の小児急性リンパ芽球性白血病（Acute Lymphoblastic Leukemia, ALL）に対する多施設共同治療研究では，単一検査施設での4カラー解析によるマーカー中央診断を行っている[1]。小児では採取できる検体量が限られていることや，貴重な余剰検体を将来の白血病治療研究のために有効活用することが今後一層重要になってくると予測されることから，マーカー検査に使用する検体量を極力押さえる努力が必要である。一方，近年の技術の進歩によりフローサイトメトリーのマルチカラー化が著しく進み，同時に多数の抗原についての情報が得ることか可能になってきている。白血病のマーカー検査についても，マルチカラー化を進めることによって，必要な検体量を減らすとともに，各抗原の発現の相互の関係がより詳細に取得できるものと期待される。そこで，今回われわれは，9カラー解析による小児白血病のマーカー解析について，その実現性と有用性に関する検討を行った。

【対象と方法】

白血病細胞株および小児ALL患児の初発時血液あるいは骨髄検体に対し，市販されているfluorescein isothyocyanate（FITC），phycoerythrin（PE），phycoerythrin-Texas Red（ECD），Peridinin Chlorophyll Protein（PerCP）またはPerCP-cyanin 5.5（PerCP-Cy5.5），PE-Cy7，allophycocyanin（APC），APC-Cy7，Pacific Blue（PB），およびCascade Yellow（CY）標識抗体を組合わせて9カラー染色を行い，CyAn ADP（3レーザー405nm / 488nm / 642nm，Beckman Coulter）により解析した。抗体は，所要量をあらかじめ混合，分注して－85度で凍結保存しておき，使用時に室温に戻して使用した。なお，予備実験により，使用直前に分注，混合した抗体を使用した場合と，あらかじめ分注して凍結した抗体を用いた場合とで，測定結果には差がないことを確認した。全血法により，PBSで洗浄して濃度調整した血液あるいは骨髄液を各チューブに添加し，室温20分反応後，赤血球溶解液で2回洗浄して，シース液に再浮遊させて測定に用いた。

細胞内抗原の染色については，あらかじめIntraPrep（Beckman）を用いて膜透過処理した細胞に，gating用の抗CD45抗体と同時に細胞内抗原染色用の抗体を添加して行なった。なお，予備実験により，膜透過処理前にCD45の染色を行なった場合と，膜透過処理後に細胞内抗原の染色と同時にCD45の染色を行なった場合とで，後者の方がCD45の発現強度が強くなる傾向を認めたものの，gatingには全く支障がなく，測定結果には差が生じないことを確認した。

モノクローナル抗体（monoclonal antibody，MoAb）のパネルは日本小児白血病リンパ腫グループ（Japanese Pediatric Leukemia / Lymphoma Study Group，JPLSG）"免疫診断委員会"の推奨検査項目を参考に選択した。ALLのマーカー解析はTCCSGの中央診断として実施しており，解析施設および検体を送付するTCCSG参加診療施設双方の倫理委員会で承認を受け，検体の送付と中央診断について，本人あるいは保護者のインフォームド・コンセントを得た上で行った。

【結　果】

抗体パネルの決定

今回は，CyAnADPはの3レーザー9カラー用モデルの標準フィルター系を使用し，入手可能（2008年9月時点）な標識抗体の組合せを考慮して，青色：25mW 488nm固体レーザーでFITC，PE，ECD，PerCP-Cy5.5 / PerCP，PE-Cy7の5色を，赤色：60mW 642nm半導体レーザーでAPCおよびAPC-Cy7を，紫色：50mW 405 nm 半導体レーザーでPB，CYを，それぞれ励起して検出する組合せとした（Table 1A）。このうち，CY標識抗体は市販品の種類が少なく，蛍光自体も弱いことから，CD45で固定し，Gating用とした。

その他の8色については，蛍光補正を容易にするため，各抗体の配色の組み合わせを工夫し，B-lineage，T-lineage，Myeloid-lineage，非-lineageの各項目が隣合うことを基本とした。特に，PE，ECD，PerCP / PerCP-Cy5.5については，小児白血病のマーカー発現において通常同時に発現することが無いか，あるいはあったとしても非常に稀なものを，隣り合うPMTチャ

[1] 国立成育医療研究センター 研究所　小児血液・腫瘍研究部
[2] 東京小児がん研究グループ
[3] 順天堂大学 小児科・思春期科
[4] ベックマンコールター株式会社
[5] 聖路加国際病院　小児科
[6] 埼玉県立小児医療センター 血液腫瘍科
[7] 東邦大学医療センター大森病院 輸血部
[8] 群馬県立小児医療センター
[9] 茨城県立こども病院

受付日：平成22年6月3日　受理日：平成22年6月21日